Effect of viscosity modifier admixture on Portland cement paste hydration and microstructure

Chaves Figueiredo, Stefan; Çopuroğlu, Oğuzhan; Schlangen, Erik

DOI
10.1016/j.conbuildmat.2019.04.020

Publication date
2019

Document Version
Final published version

Published in
Construction and Building Materials

Citation (APA)
Chaves Figueiredo, S., Çopuroğlu, O., & Schlangen, E. (2019). Effect of viscosity modifier admixture on Portland cement paste hydration and microstructure. *Construction and Building Materials*, *212*, 818-840. https://doi.org/10.1016/j.conbuildmat.2019.04.020

Construction and Building Materials 212 (2019) 818–840

Contents lists available at ScienceDirect

Construction and Building Materials

journal homepage: www.elsevier.com/locate/conbuildmat

Effect of viscosity modifier admixture on Portland cement paste hydration and microstructure

Stefan Chaves Figueiredo *, Oğuzhan Çopuroğlu, Erik Schlangen

Microlab, Faculty of Civil Engineering and Geosciences, Delft University of Technology, Delft 2628, CN, The Netherlands

HIGHLIGHTS

- VMA concentration significantly influences Portland cement hydration.
- HPMC contributes to increase the cement paste hydration degree, as this material works as water reservoir during the curing.
- Anomalous growth of some hydration products was observed when HPMC was used.

ARTICLE INFO

Article history:
Received 31 October 2018
Received in revised form 31 March 2019
Accepted 4 April 2019

Keywords:
Viscosity modifier
Microstructure
Additive manufacturing
3D printing
Extrusion

ABSTRACT

Significant attention has been given to the development of new materials and techniques to be employed in the construction market. One of the techniques which has drawn noticeable attention is the additive manufacturing process (a.k.a. 3-dimensional printing (3D printing)). One of the approaches of this construction technique is the extrusion of cementitious composites to form contour of a desired geometry. To achieve high viscosity in cementitious materials, usually viscosity modifying admixtures (VMA) are employed. However, the consequences of using these admixtures at high dosages is still not fully understood. This study characterized the influence of different VMA dosages on Portland cement paste, through a microstructure analysis. Hydration development was assessed, and effect of the admixture was quantified at different curing ages. Techniques such as thermogravimetric analysis, optical and electron microscopy, X-ray diffraction, Fourier transform infrared spectroscopy, micro computed tomography scan and nanoindentation were employed. Important negative side effects were found such as: VMA increasing the cement setting time, anomalous dispersion of hydration products in the bulk and increasing the void content. On the other hand, positive effects were also found such as: evidence of internal curing, higher degree of hydration and lack of undesired hydration products.

1. Introduction

A promising construction technique which has drawn notable attention in the past few years is the additive manufacturing (AM). This revolutionary technique is likely to open a new era in the construction industry, optimizing process and materials [1]. AM is a general classification for technologies which fabricates objects with the help of automated equipment, directly from a digital design technology [2,3]. There are several different techniques to manufacture the objects developed based on AM, such as the powder bedding with an inkjet head [4] or the laser melting [5], and the counter craft technology which employs extrusion techniques to fabricate objects [6]. Both AM technologies build as object through a layer by layer deposition process. The countercraft AM has drawn a lot of attention in the construction market as its implementation looks feasible to be applied in large scale. It should be noted that materials with unique properties need to be developed to meet the mechanical and durability-related requirements of a long-lasting and safe structure.

Recent investigations have shown the development of cementitious composites with different aggregate particle sizes. Concrete and mortars have been developed with printable characteristics. In some studies fibres have been incorporated to stabilize the mixture at fresh state or to minimize the occurrence of cracks due to shrinkage. However, the materials and printing methods have not yet delivered solutions to improve the hardened performance of composites when loaded in tension [7,8].

Moreover, researchers have addressed this problem developing a technique to produce mortar filaments through AM reinforced by

* Corresponding author.
E-mail address: S.ChavesFigueiredo@tudelft.nl (S. Chaves Figueiredo).

https://doi.org/10.1016/j.conbuildmat.2019.04.020
0950-0618/

a steel wire. Higher ductility was achieved with samples reinforced by the steel wire. Further, more research is needed to enhance the interface bonding between the wire and the mortar [9].

Another strategy to increase the ductility of printed brittle materials is fibre incorporation. Great plastic deformations can be achieved on cementitious composites reinforced by fibres, namely strain hardening cementitious composites (SHCC). This type of composite can deliver high tensile strain, strength and frequent but tiny multiples cracks under tensile loading [10].

SHCCs are cementitious composites reinforced by high volume of fibres. Usually the reinforcement level is around 2% of the total composite's volume, which brings challenges regarding the flowability of such mix designs. An alternative often approached to enhance the fibre dispersion is the employment of viscosity modifier admixtures (VMA) [11,12]. These admixtures are usually composed of long organic chains with -OH ramifications, that arrest the free water in the mixture through hydrogen intermolecular bridge. One of the most used VMA is composed of hydroxypropyl methylcellulose (HPMC) [13]. In addition, the use of VMA is a key factor when developing printable cementitious composites [12]. The adjusting of the amount of the chemical admixture, coupled with a good distribution of particles grain size in the matrix, and optimum water-to-solid ratio may lead towards a material with the needed viscosity for printing.

Khyat detailed several types of VMA that can be used in cementitious materials. The author separated them in five different classes according with the mechanism of action and their composition. In general they are employed in the construction industry to control some of the fresh state properties for development of high performance cementitious composites, such as specific types of grouts or under water projects [14]. Furthermore, other studies have demonstrated the ability of VMAs to arrest the water available in cementitious mixtures. For instance, the employment of HPMC in some cement-based mortars enhances significantly their water retention improving or keeping the quality of this type of material inside certain limits [15–18]. Moreover, D. Marchon *et. al.* approached the need to control rheological properties of fresh cementitious mixtures to be applied for 3D printing. In that article several different types of admixtures are discussed and the importance of VMAs for the pumping, extrusion and deposition phase of printed cement-based composites is acknowledged [19]. Thus, the use of VMAs in the construction industry helps concrete technologists to keep viscosity and yield stresses of mixtures under control.

Besides the fact that VMA can help in controlling the rheological properties of a solid suspension, the consequences on the microstructure of hydrated Portland cement is not yet fully understood. The influence of some water-soluble polymers on the microstructure development of Portland cement was investigated in [20]. Their findings showed a delay on the hydration process, formation of unusual minerals at early ages, a slightly lower Ca $(OH)_2$ content and a higher amount of chemically bounded water. Besides that, a higher cohesion of the cement paste resulting in a lower number of microcracks and different morphology of portlandite crystals was also observed under microscope.

Researches investigated the influence of HPMC with different viscosities in the hydration of two individual phases of the Portland cement clinker. They demonstrated through calorimetry measurements that independently of VMAs viscosity the hydration of C_3S and C_3A was delayed with the use of rheology modifier admixture. Nevertheless, blending each individual phase with gypsum would lead towards a slightly different result. Naturally, the addition of gypsum delayed hydration of both phases as it would happen in an ordinary Portland cement hydration. However, reactions of blended C_3A and gypsum powders were sensitive to VMA viscosity. The authors justified their finds stating that C_3A hydration was more susceptible to lower ions mobility through viscous solutions [21].

Furthermore, the cement hydration delay was explained with the effect of HPMC on the precipitation of calcium hydroxide, the polymer's water absorption capacity [22–24], and the methyl

Table 1
Chemical composition of Portland Cement used in this study.

Compound	CEM I 42.5 N [%]
CaO	69.53
SiO_2	15.60
Fe_2O_3	3.84
Al_2O_3	3.09
SO_3	2.60
MgO	1.67
K_2O	0.55
TiO_2	0.31
P_2O_5	0.14
Rest	0.53
LOI	2.14

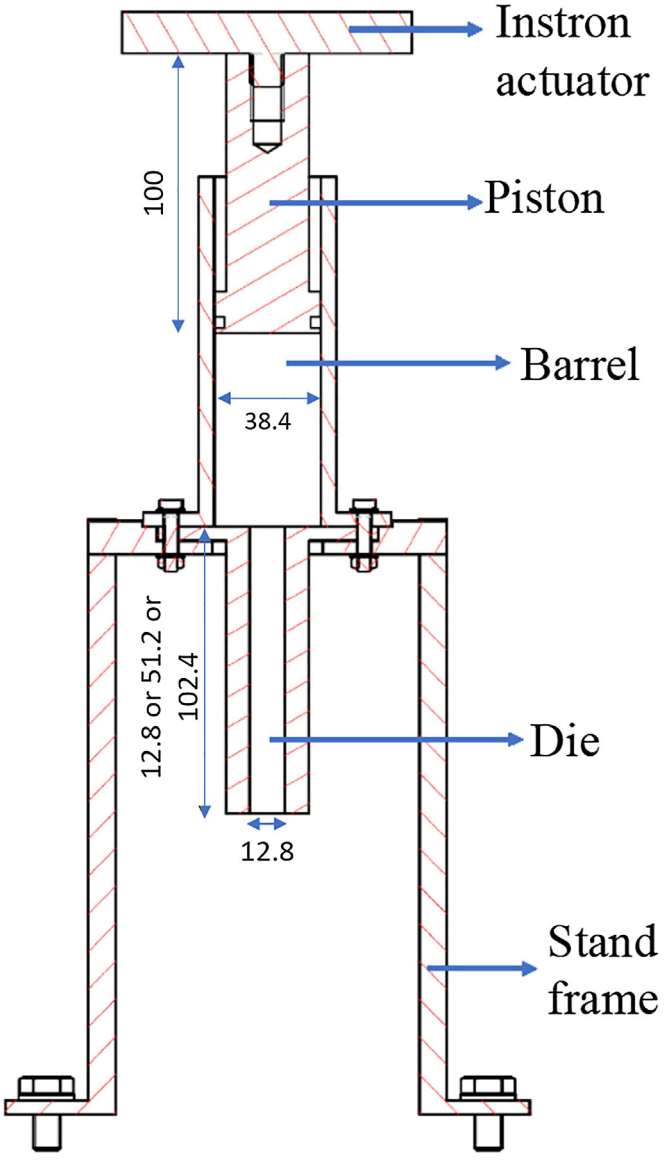

Fig. 1. Ram extruder and its components (dimensions are in millimetres).

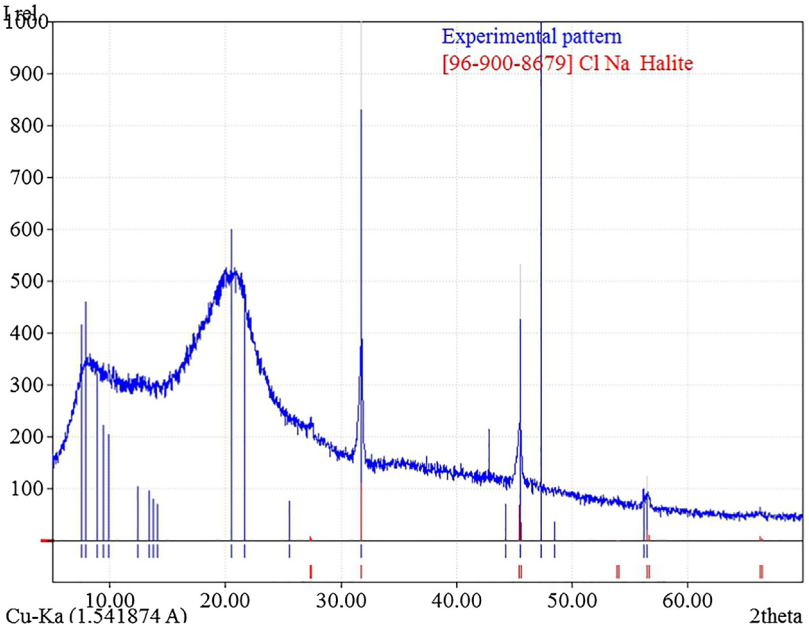

(a) XRD pattern obtained from HPMC showing the NaCl impurity

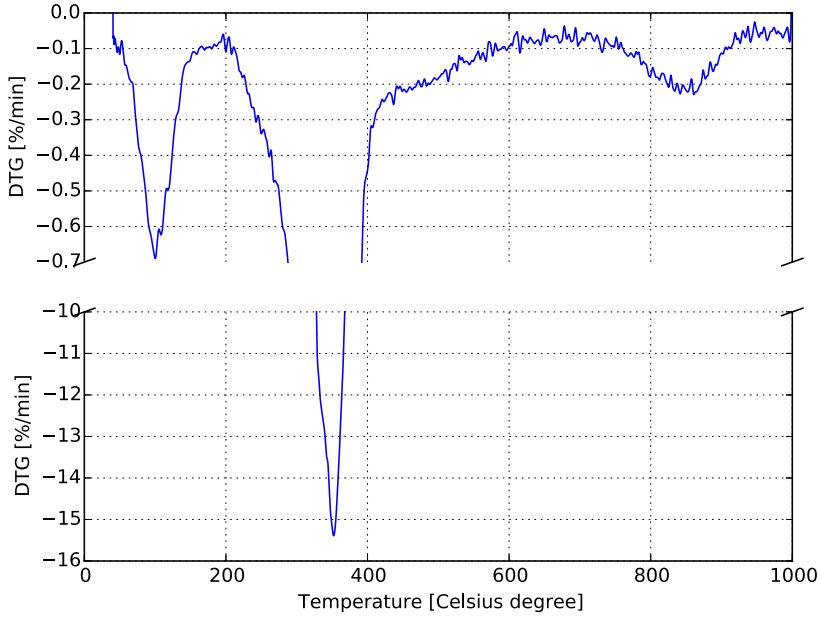

(b) DTG results from the HPMC

Fig. 2. HPMC Impurity characterization.

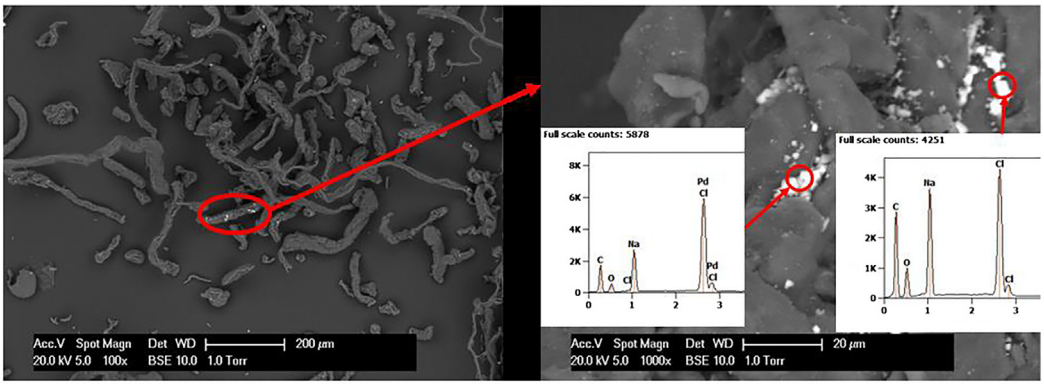

Fig. 3. Electron microscope image and chemical composition from EDS measurement.

content [25]. Moreover, a study have also reported the influence of molecular weight on the rheology of cement paste modified by HPMC admixture and its potential to combine via intermolecular and intramolecular crosslinks with Ca^{+2} ions [26]. This study also reports potential challenges using HPMC together with polycarboxylate superplasticizers as HPMC molecules have the potential to adsorb superplasticizer molecules. Hence, the probability of SP molecules to be deposited in te surface of the cement particles decreases.

As demonstrated by other studies and summarized here, the employment of VMAs to control rheological properties of cementitious materials is essential to the development of printable mixtures. However, the consequences of using this organic admixture in the microstructre of cement-based materials is not

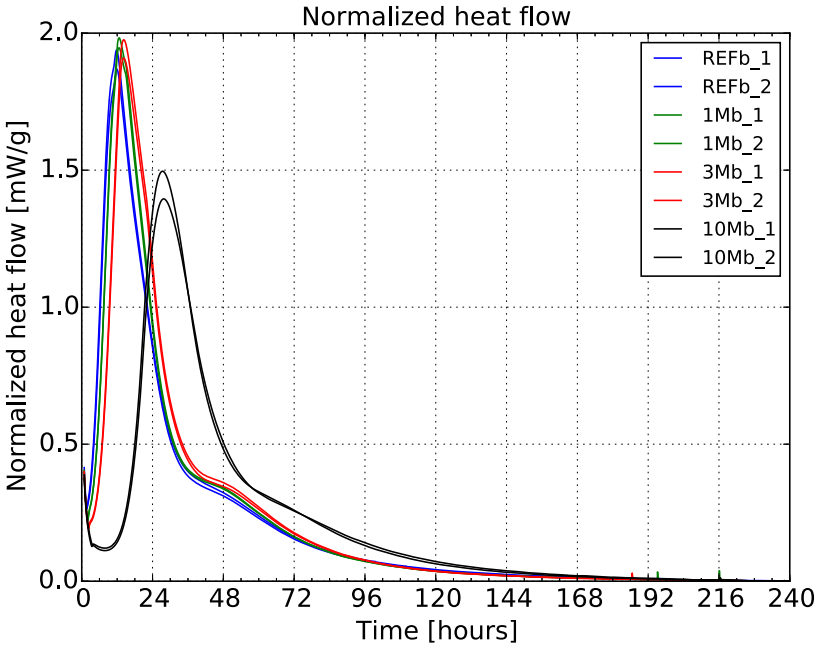

(a) Normalized heat flow

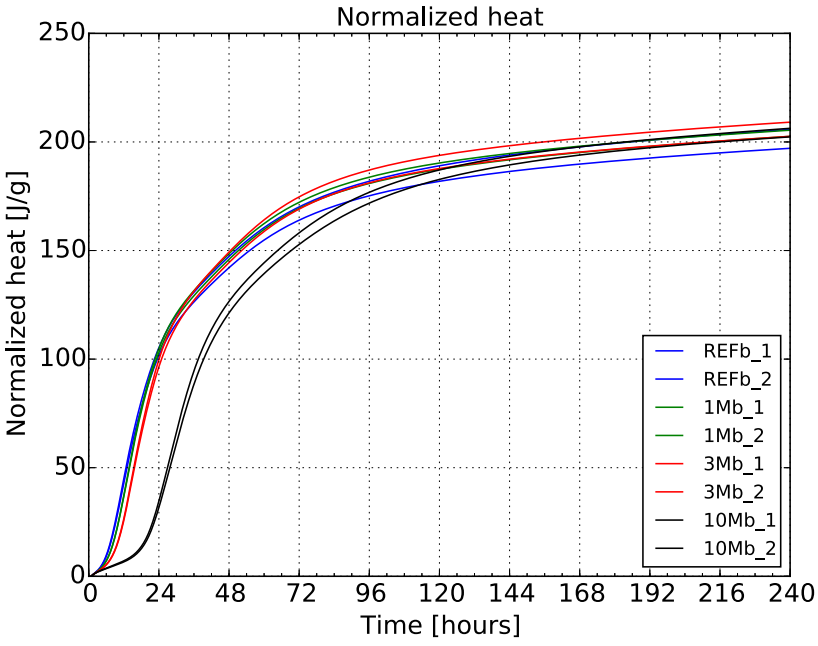

(b) Normalized heat flow

Fig. 4. Isothermal calorimetry test from the initial 10 days of hydration.

Table 2
Summary of properties measured using TGA technique.

	Age [days]	α	H_2O from 105 to 450 °C [%]	Portlandite [%]	Calcium carbonate [%]	Portlandite before carbonation [%]
REF	1	0.2932 ± 0.0112	4.12 ± 0.21	7.64 ± 0.05	5.12 ± 0.03	10.61 ± 0.07
	2	0.3745 ± 0.0073	5.33 ± 0.01	7.58 ± 0.34	5.44 ± 1.16	10.80 ± 0.52
	3	0.4081 ± 0.0027	5.79 ± 0.08	7.93 ± 0.06	5.52 ± 0.68	11.22 ± 0.45
	29	0.6489 ± 0.002	8.88 ± 0.11	11.79 ± 0.97	5.43 ± 0.03	15.07 ± 0.99
1 M	1	0.3472 ± 0.0159	4.86 ± 0.06	8.09 ± 0.12	5.76 ± 0.71	11.55 ± 0.41
	2	0.4192 ± 0.0167	5.55 ± 0.16	9.44 ± 0.89	5.86 ± 0.59	12.99 ± 0.45
	3	0.4327 ± 0.0065	5.90 ± 0.16	8.40 ± 0.52	7.65 ± 1.64	13.29 ± 0.71
	7	0.5584 ± 0.0145	7.46 ± 0.14	9.51 ± 0.26	7.40 ± 0.32	14.23 ± 0.49
	29	0.734 ± 0.0118	9.43 ± 0.04	12.73 ± 0.81	8.49 ± 1.13	18.29 ± 0.04
3 M	1	0.3311 ± 0.0094	4.70 ± 0.12	6.87 ± 0.35	6.92 ± 0.75	11.19 ± 0.21
	2	0.4218 ± 0.0096	5.72 ± 0.02	8.32 ± 0.16	6.74 ± 1.09	12.53 ± 0.97
	3	0.4972 ± 0.0077	6.55 ± 0	9.47 ± 0.22	6.56 ± 0.94	13.56 ± 0.48
	7	0.611 ± 0.0019	8.02 ± 0.08	11.08 ± 1.32	6.47 ± 1.15	15.12 ± 0.46
	29	0.7838 ± 0.03	10.07 ± 0.1	14.41 ± 0.8	6.19 ± 1.49	18.27 ± 0.31
10 M	1	0.1472 ± 0.0069	2.17 ± 0.02	1.30 ± 0.25	5.44 ± 0.15	4.49 ± 0.35
	2	0.3238 ± 0.008	4.49 ± 0.08	5.70 ± 0.31	8.07 ± 0.16	10.88 ± 0.19
	3	0.4403 ± 0.0017	5.90 ± 0.11	8.51 ± 0.62	8.84 ± 2.32	14.28 ± 1.11
	7	0.5503 ± 0.0092	7.19 ± 0.01	9.44 ± 0.48	13.04 ± 1.13	18.35 ± 0.36
	29	0.7353 ± 0.0423	9.36 ± 0.23	13.45 ± 0.61	10.86 ± 1.98	20.77 ± 0.88

clear. The present research aims to build a better understanding to the consequences of HPMC use in cement paste. This information together with the literature already available, contributes to the new generation of construction materials which are under development to be applied on 3D printing.

2. Experimental methods

Chemical composition of the Ordinary Portland Cement (OPC) CEM I 42.5 N and its loss on ignition (LOI) can be found in Table 1. They were assessed by X-ray fluorescence analysis (XRF) and thermogravimetric analysis performed at 10 K/min under Argon atmosphere. The LOI was determined using the loss of mass between 45 and 1000 °C.

The VMA used for this study is composed by HPMC with viscosity of 201,000 mPa.s. The samples were cast mixing a volume of 0.5 litres in a planetary mixer according to the following procedure:

- All dry materials were mixed for two minutes at low speed (speed 1–60 rpm);
- While mixing at speed 1, during approximately two minutes, the water was added;
- The wet powders were mixed during the next two minutes at speed 1. In this phase it was possible to observe a significant change in the mixture's viscosity. A dough like consistence was achieved;
- Using a spoon the wet powder is manually mixed, in order to ensure a homogeneous mix;
- At high speed (speed 2–124 rpm), the dough like cement paste was further mixed. At this phase the rigid dough becomes softer and "opens" in the mixing bowl.

A reference cement paste with a water-to-cement (w/c) ratio of 0.3 (REF) and three levels of VMA, 0.1, 0.3 and 1% of the cement mass, named 1M, 3M and 10M respectively were evaluated. The VMA content employed in this study follows the same levels found in [12] where the rheology of crowded solid suspensions using this type of admixture was studied, aiming the development of printable SHCCs.

The mixed paste was cast inside plastic containers (33 mm diameter ad 69 mm height) and sealed with the help of paraffin paper. Right after moulding they were left for 24 h rotating around their own axis (5–7 rpm), as reported by [27], to ensure a homogeneous material avoiding any segregation and bleeding, as discussed in [28]. With the exception of 10M samples, afterwards, they were demoulded and cut in slices of approximately 5 mm and cured at (20 ± 2) °C and relative humidity of (98 ± 2)%. 10 M samples could only be demoulded and cut 48 hours after casting.

To stop cement hydration the cut slices were manually crushed into small pieces and partially submerged in liquid nitrogen for 3 minutes and completely submerged for 5 minutes. Immediately after, crushed particles were conditioned in plastic bags with holes to allow the release of moisture from the samples and stored in a freeze drier for further drying. Those samples were used for thermogravimetric analysis (TGA). The small cut slices destined to electron microscopy observations, X-ray diffraction (XRD), Fourier Transform Infrared Spectroscopy (FTIR), micro Computed Tomography scan (Micro-CT scan), nanoindentation and thin section microscopy observations had their hydration arrested by solvent exchange procedure, employing ethanol [29]. To investigate the hydration progress of all samples the following procedures were used for each test:

- Thermogravimetric analysis (TGA):

The test was performed increasing the temperature from 40 to 1000 °C at 10 K/minute. In order to quantify the hydration products and total degree of hydration the mass loss was measured according with the following thresholds:

- 110 °C to 450 °C: water loss from AFm products;
- 450 °C to 520 °C: water loss from portlandite;
- 550 °C to 800 °C: carbon dioxide loss from calcium carbonate minerals.

Portlandite and calcium carbonate contents were measured taking the stoichiometry balance of each reaction into account. Moreover, the total degree of hydration was calculated deducting the mass loss from the calcium carbonate minerals. Two tests were run for each sample. Additionally, a TGA test only with pure VMA was run to quantify the mass loss of different temperatures. This test was important for adjustments on samples where HPMC was employed.

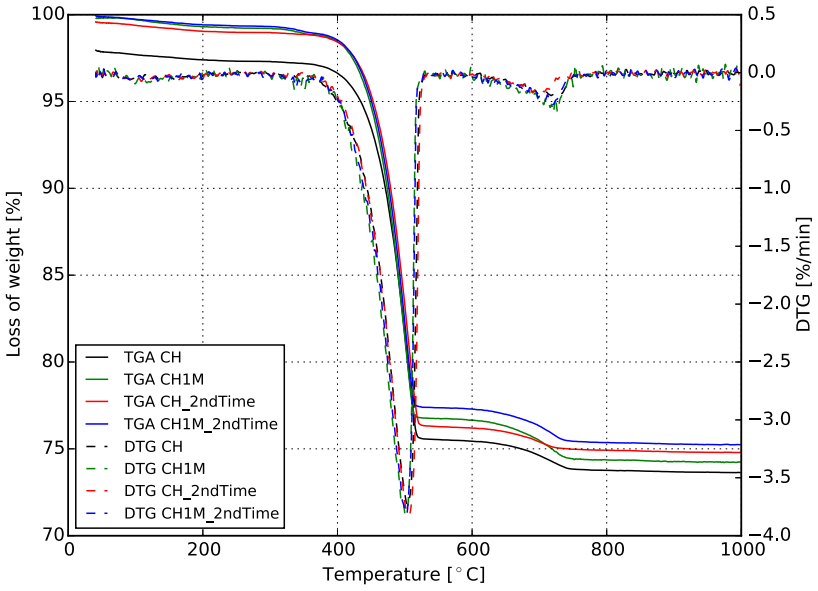

(a) TGA and DTG curves

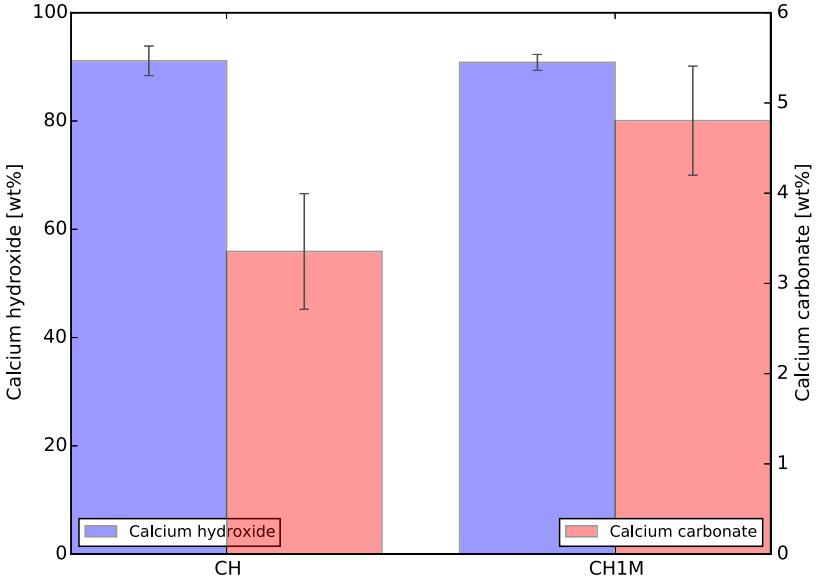

(b) Calcium hydroxide and calcium carbonate average content

Fig. 5. Summary of results found in the calcium hydroxide experiment.

- X-ray diffraction (XRD) and Fourier Transform Infrared Spectroscopy (FTIR):

  Powder samples analysed with the XRD and FTIR were hand milled to avoid heating up the samples. The materials used in both tests were sieved with a 75 µm opening sieve. XRD samples were measured from 2θ equal to 5° to 70°, at 2°/min. FTIR samples were tested measuring bands from 550 to 4000 cm^{-1}.

- Isothermal calorimetry analysis:

  The total energy in form of heat released during the first 10 days of cement hydration was measured with the assistance of a TAM Air Isothermal Calorimeter with eight channels, at 20 °C and using as reference ampoules with sand. The samples used for this test were mixed outside of the calorimeter. Therefore, the initial peak of heat released corresponded to the exothermic dissolution of the grains and formation of first AFt phases were not present in these results.

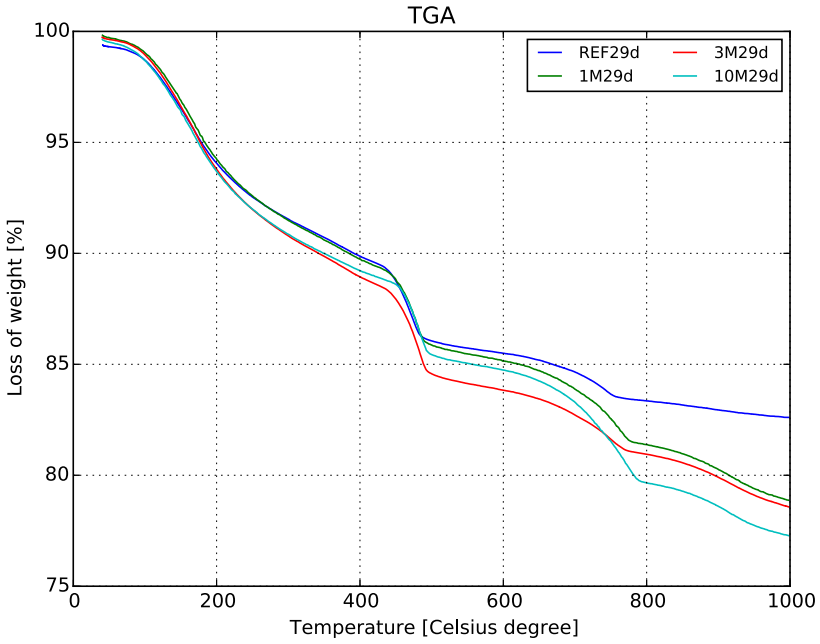

(a) TGA

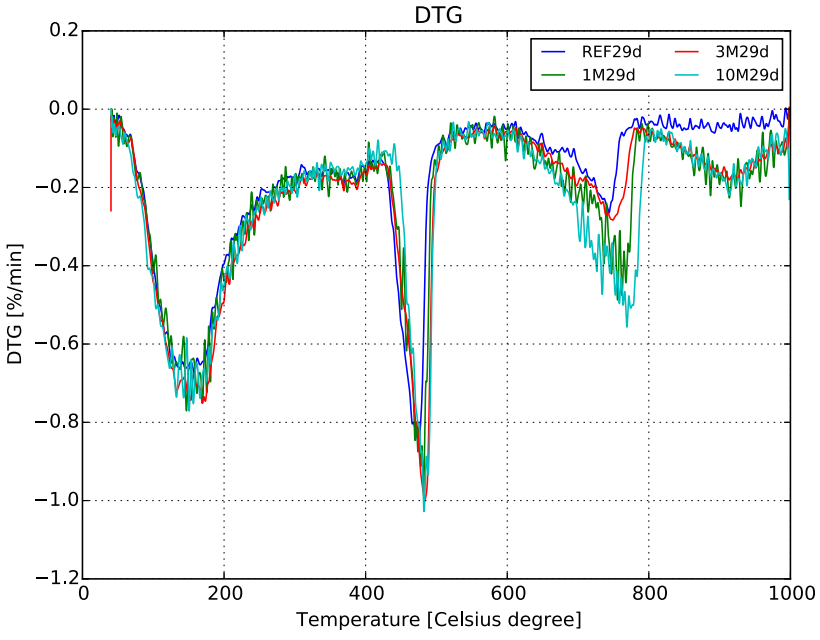

(b) DTG

Fig. 6. Thermogravimetric results from 29 day-old samples.

- Thin section analysis:

Thin section specimens otherwise known as "petrographic thin section" were produced for all four mixtures, from specimens which had its hydration arrested by solvent exchange. A thin section sample had approximately 30 μm thickness and it was obtained through a controlled grinding process employing a semi-automatic thin section machine where three rollers with diamonds of 64, 46, 16 μm were used. Low viscosity epoxy with fluorescent pigment was used to guarantee sample stability during preparation and facilitate porosity investigations under ultra-violet (UV) light. Thin section samples were observed with a Leica DM2500P polarized light microscope equipped with linear and circular polarization filters. Lenses of 2.5×/0.07, 10×/0.22 and 20×/0.4 (magnification/numerical aperture) were available. Plane polarized light (PPL), PPL with UV light, cross

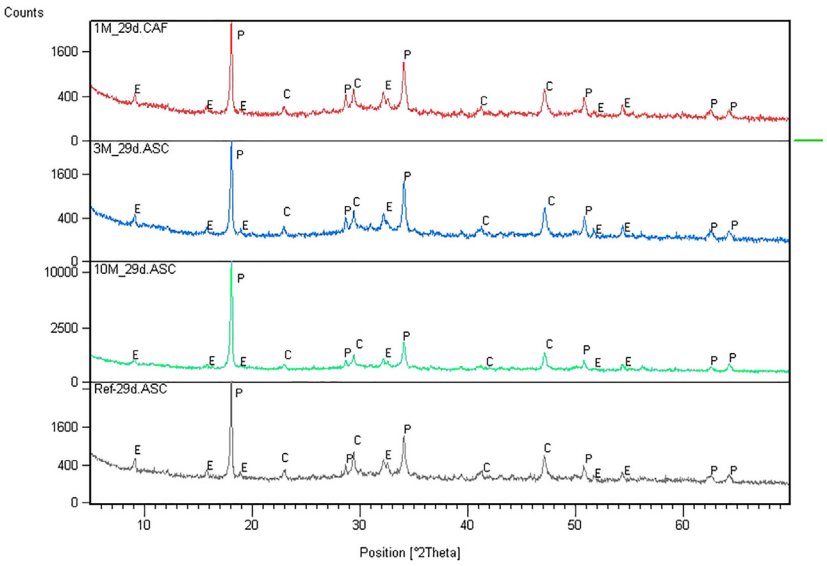

Fig. 7. XRD pattern of samples with 29 days, where ettringita (E), calcium carbonate (C) and portlandite (P) peaks are in evidence.

polarized light (XPL) and circular polarized light (CPL) were used to observe the air entrapped voids and the portlandite distribution in the paste. The advantages of using CPL for quantitative image analysis have been shown in [30]. Using this technique all available portlandite crystals can be observed in a single field of view, in contrast with XPL where only a portion of the available crystals are visible due to the extinction phenomenon.

- Scanning electron microscope (SEM):

Samples destined to SEM observations were mounted in a working glass and ground with the help of a thin section grind machine with the same three rollers employed for manufacturing of thin section samples. These samples were also impregnated using a low viscosity epoxy with epo-dye colour and had their surfaces ground and polished. To ensure the thickness of epoxy on the surface of the sample, they were measured before and after epoxy impregnation. After epoxy impregnation, the samples were ground again only with the roller with 16 μm diamonds. Only after ensuring a flat surface, the samples were ground employing the 1200 silicon carbide paper cooled with ethanol. For polishing purposes, a paste with 6, 3, 1 and 0.25 μm diamonds were used. Back scattered electrons (BSE) and secondary electrons (SE) images were obtained.

In order to quantify information which can contribute to the understanding of the hydration development, image analysis with the help of Trainable Weka Segmentation tool [31] from FIJI [32] was performed. 30 images with 200 times magnification covering a total area of 214.03 mm^2 was used per mixture. The average area of unhydrated OPC particles, inner and outer products, portlandite and voids were measured.

- Micro computed tomography scanner (Micro-CT scan)

To obtain the average size and the total volume of voids on the analysed pastes with VMA a Phoenix Nanoton m Micro-CT scanner was employed. Cylindrical specimens with 35 mm diameter and approximately 3 mm height were scanned, reaching 16.67 μm/pixel resolution. Afterwards, an image stack with the top view of the cylinder was analysed with the help of Trainable Weka Segmentation tool [31] from FIJI [32]. For those images, only two phases were distinguished voids and matrix.

- Mechanical performance (Nanoindentation and compressive strength)

The mechanical performance of the studied pastes were assessed through compressive strength of cubes with 40 mm edges at 2, 3, 7 and 29 day-old of curing and nanoindentation of 29 days-old samples.

To quantify the matrix stiffness a nanoindenter MTS G200 with continuous stiffness measurement was used. This measurement was employed to investigate the local mechanical performance of the paste and quantify the influence of VMA at this scale. The surface of the samples tested through this technique were flat and scratch free. To achieve this surface quality a similar approach as the one employed in the sample preparation dedicated for specimens investigated under SEM was used with exception of the epoxy impregnation step. The polishing done in the lapping table using diamond paste with 6, 3, 1 and 0.25 μm diamonds and cooled with ethanol was executed for 10, 10, 15 and 30 minutes for each specimen respectively. After polishing the samples were stored in a vacuum oven at 25 °C before testing. A grid of 15 × 15 indents were made using a strain ratio of 0.05/s until the maximum depth of 2000 nm. The indents were separated of each other by a distance of 50 μm. In order to calculate the average stiffness of each indent the Poison ratio of 0.2 was used and the values were calculated from a depth of 200 to 400 nm. Hydration products were identified by their stiffness as reported in [33,34].

- Rheological properties

The rheology properties are very important to define a printable mixture. Materials developed for printing purposes must be stable under high pressures to avoid any type of segregation when the mixture is under pressure and they must also have shape stability in order to manufacture the desired

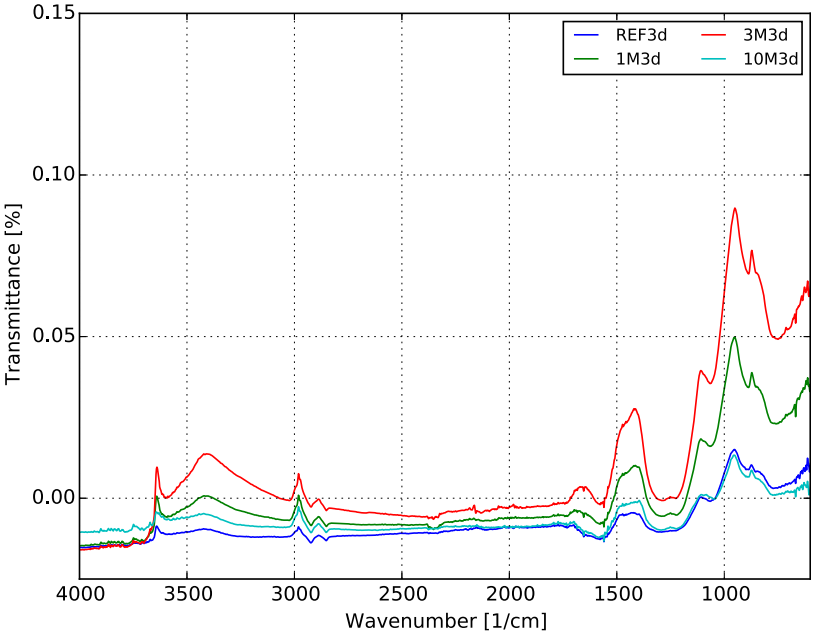

(a) 3 days

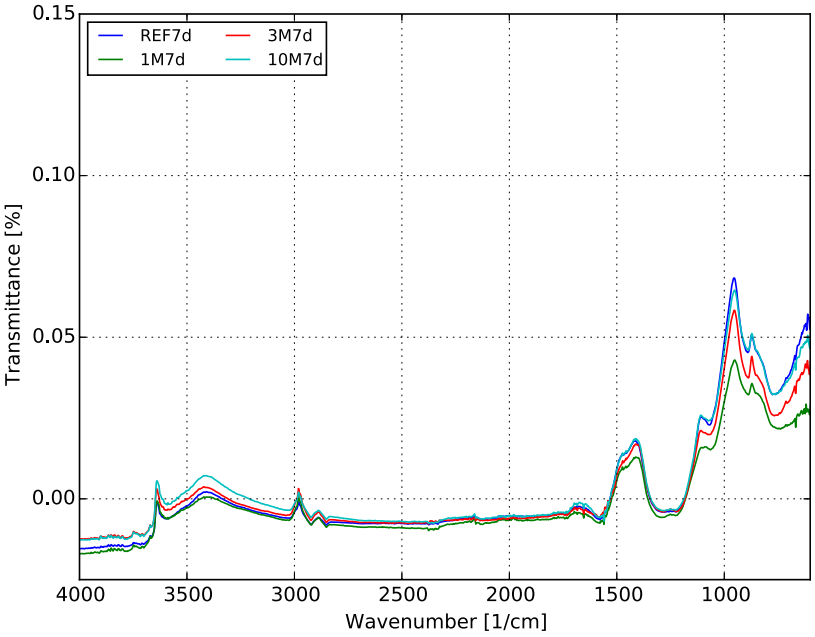

(b) 7 days

Fig. 8. FTIR results.

contour. All those empirical parameters needed for a printable mixture were quantified by means of rheological tests. For this study, a ram extruder (Fig. 1) was employed to assess the paste rheology parameters. Three dies with a length-diameter ratio of 1, 4 and 8 plus, four different extrusion speeds 0.25, 0.5, 1 and 2 mm/s were employed. Using six parameters analysis from the Benbow-Bridgewater (Eq. 1) model the properties which governs the flow of this type of solid suspension were obtained. The parameters "m" and "n" are responsible to guarantee the non linear behaviour of the pressure drop with the extrusion speed characteristic from pseudo-plastic fluids.

$$P = P_1 + P_2 = 2\ln\left(\frac{D}{d}\right)(\sigma_0 + \alpha V^m) + \frac{4L}{d}(\tau_0 + \beta V^n) \quad (1)$$

Where:

P = Total pressure drop [kPa]
P_1 = Pressure drop in the die entry [kPa]
P_2 = Pressure drop in the die land [kPa]
σ_0 = Bulk yield stress [kPa]
α = Parameter characterizing speed in the die entry [kPa.s/mm]
V = Extrusion speed in the die land [mm/s]
D = Barrel diameter [mm]

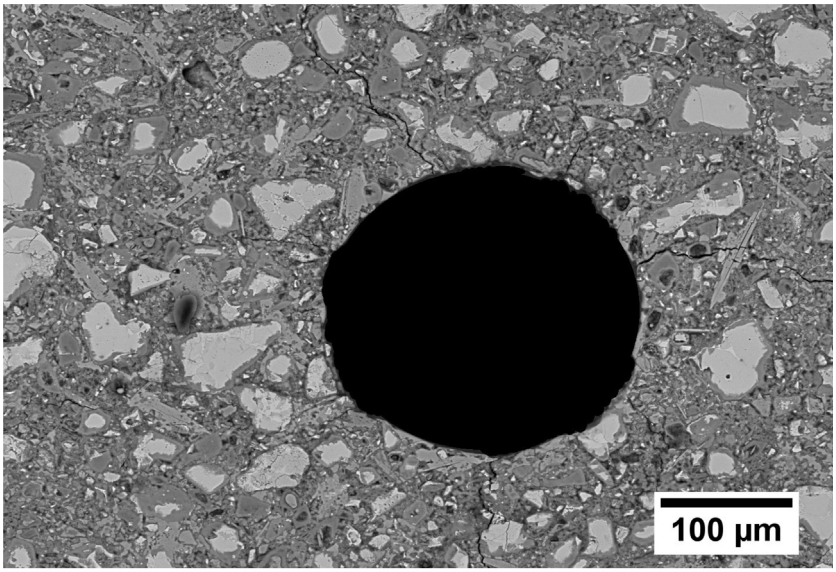

(a) REF

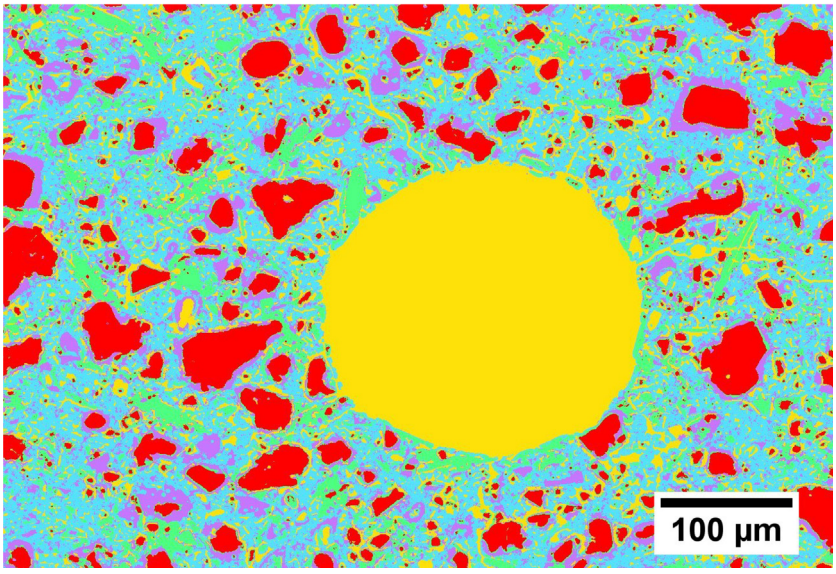

(b) REF + Weka segmentation

Fig. 9. SEM picture from REF sample with 29 days of curing and the result from the image analysis.

d = Die diameter [mm]
τ_0 = Shear yield stress [kPa]
β = Parameter characterizing speed in the die land [kPa.s/mm]
L = Die length [mm]

3. Results

Before the description of all results found for evaluated specimens it is important to show that the VMA employed was investigated under electron microscope, TGA and XRD. The results from these tests have demonstrated that the chemical admixture suffers from sodium chloride impurity. The impurity was found through TGA from the weight loss from 800 to 950 °C, as shown on the differential thermogravimetry (DTG) curve plotted in Fig. 2(b). At this interval of temperature halite melts and small portions of it might vaporize, as demonstrated by the loss of mass. XRD pattern plotted on Fig. 2(a) also shows the presence of NaCl crystals, among all the amorphous organic phase. Finally, as shown in Fig. 3 the salt crystals were observed using an Environmental SEM, and with the help of Energy-Dispersive X-ray Spectroscopy (EDS) measurements the presence of peaks of sodium and chlorine were found. It should be noted that NaCl accelerates OPC hydration [35,36], and leads to corrosion of steel reinforcement [37,38].

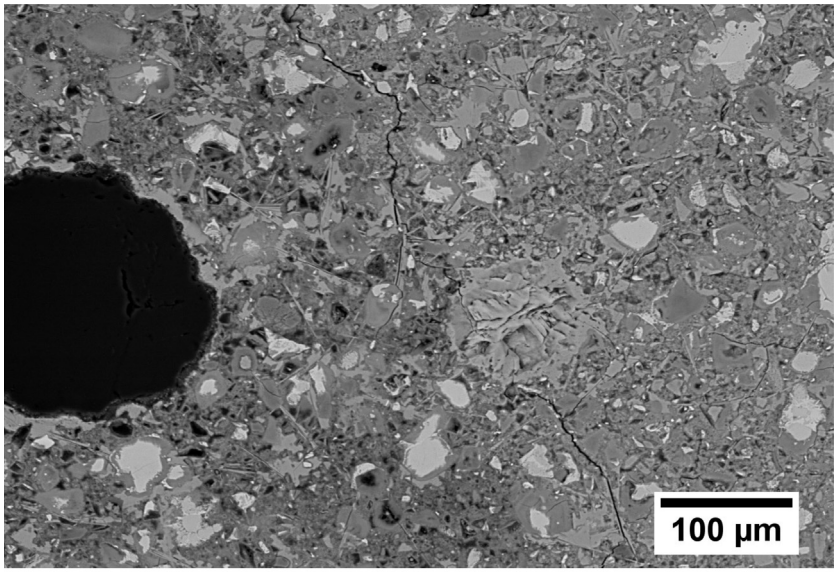

(a) 1M

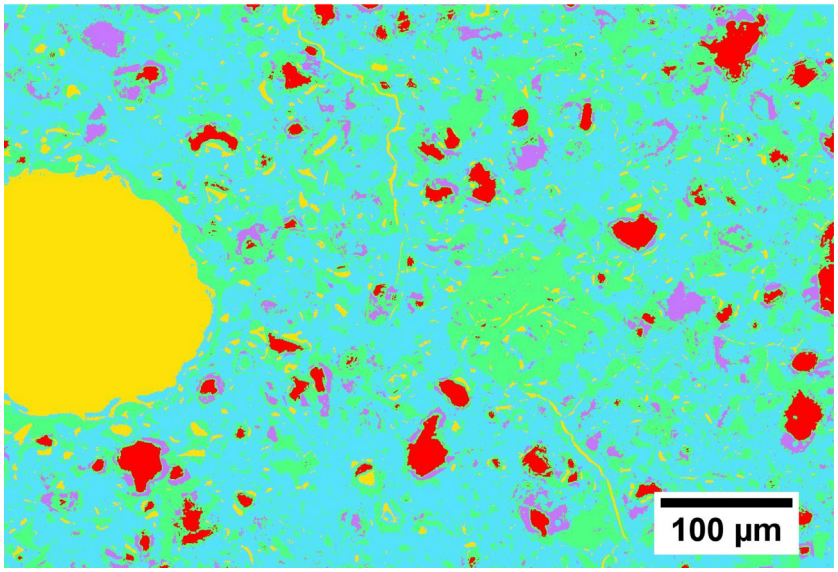

(b) 1M + Weka segmentation

Fig. 10. SEM picture from 1 M sample with 29 days of curing and the result from the image analysis.

3.1. Isothermal calorimetry test

In Fig. 4 the result from the isothermal calorimetry test was reported. The increasing volume of viscosity modifier on the cement paste, lead towards delaying Portland cement hydration. The greatest consequences were measured on pastes with 1% of VMA, where the dormant stage went up to the first 9 hours of hydration.

Specimens 1M and 3M had also their early age properties changed. Both had a slightly longer dormant period, than the reference as also reported by [21]. However, the C_3S peak obtained for both was also slightly higher than reference samples, meaning that the hydration reactions were significantly accelerated after the extended dormant period. Other fact that shows this acceleration is the overlapping of the peak of heat generated by the hydration of C_3S and the renewed formation of ettringite [39]. In reference samples after about 10 hours the slope of the heat release decreases, followed by a re-acceleration after some minutes. In 1M samples the different slopes can also be noticed however, the second slope was shown only during the descending part of the curve, after approximately 10.5 hours. Specimens with 0.3% of VMA do not show these two slopes. The heat released by these clinker components overlay creating a wider peak.

In Fig. 4(a) the total heat generated during the measurement period was plotted. Besides the fact that the employment of VMA delays Portland cement hydration, after approximately 30 hours of hydration samples 1M and 3M had already a slightly higher total heat released. In general, samples with HPMC have released a higher amount of energy during the first 10 days of curing.

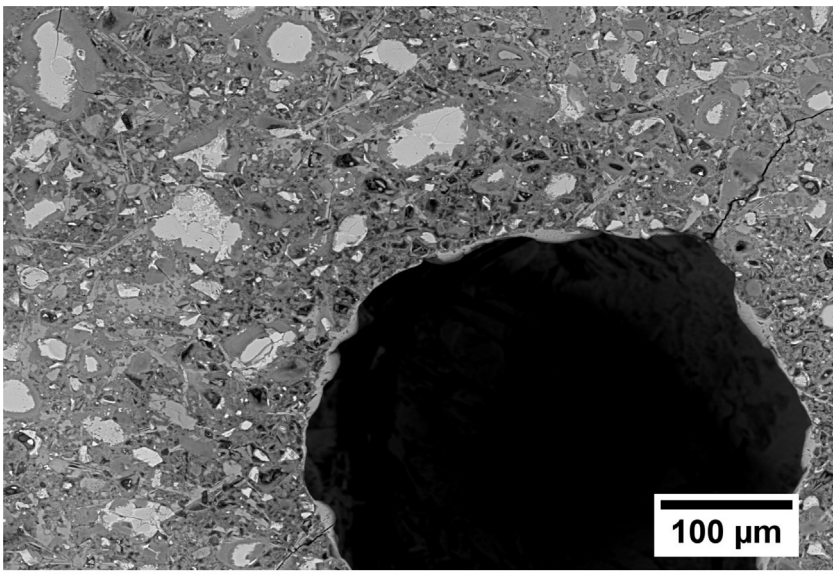

(a) 3M

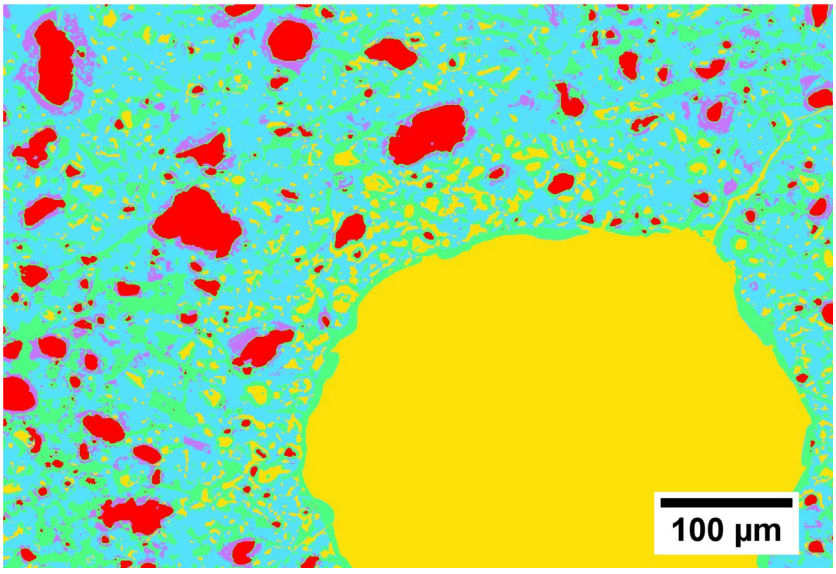

(b) 3M + Weka segmentation

Fig. 11. SEM picture from 3 M sample with 29 days of curing and the result from the image analysis.

3.2. Thermogravimetry analysis

Thermogravimetry results were especially important to quantify the results found on this study. A summary with all results obtained with the test is given in Table 2. The influence of 1% VMA on the hydration delay of cement paste could also be noticed on the TGA results. Degree of hydration (α) was calculated for all samples and the results show a significant loss on 1 day cured samples for 10M specimens. Moreover, a significant increase in α since the 1st day of hydration for 1M and 3M specimens was noticed. 10M specimens only develop higher degree of hydration after the 3rd day.

To explain the higher values found for samples with HPMC an understanding of how this chemical admixture changes the viscosity of solid solutions must be approached. The HPMC molecules are able to 'arrest' water through hydrogen intermolecular interactions. These interactions decrease the availability of water during the first hours of cement hydration increasing significantly the viscosity of the water which surrounds OPC particles. As soon as pore solution pH rises, the increasing availability of OH^- ions decreases the capabilities of VMA in change the viscosity of the solid suspension by rescuing the kidnapped water molecules and making water molecules available for hydration again. Gradually this phenomenon happens in the paste, and therefore gradually the water 'arrested' on HPMC molecules are released to become available for hydration. This description is also found to explain the phenomenon known as internal curing. Therefore, it is believed that

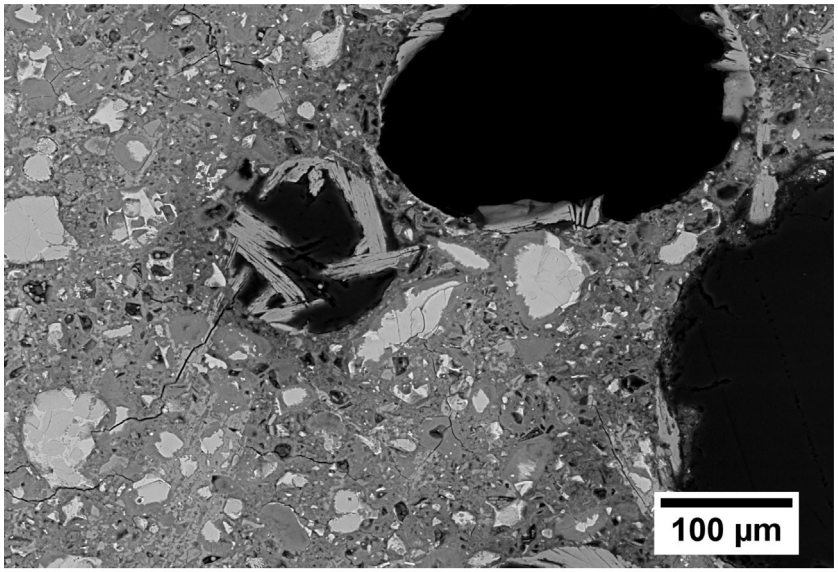

(a) 10M

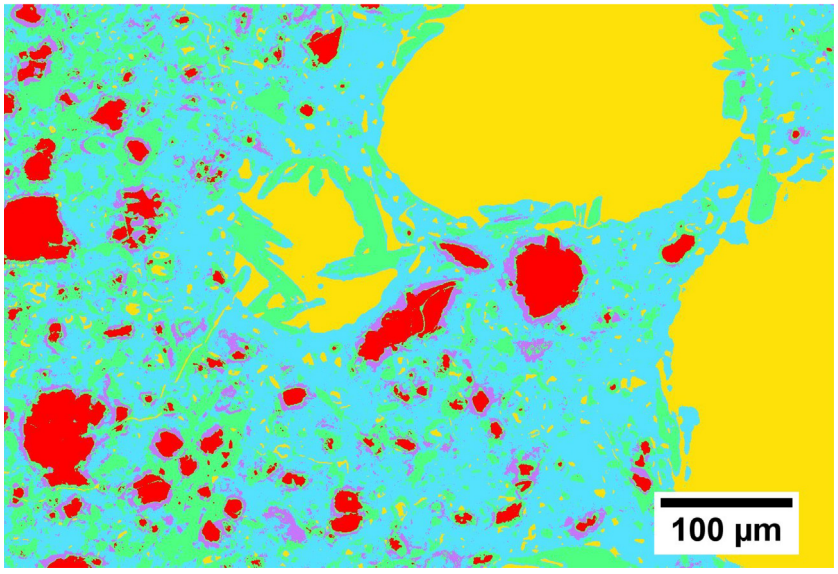

(b) 10M + Weka segmentation

Fig. 12. SEM picture from 10 M sample with 29 days of curing and the result from the image analysis.

the VMA does not only contribute to the viscosity modification of the solid suspension, but also to improve OPC hydration.

The mechanism which VMA provides internal curing to the cement paste is very similar to the ones reported to other materials with equivalent water retention, such as natural fibres [40,41], super absorbent polymers [42] or porous aggregates [43,44].

The total loss of water from AFm and CSH, as well as the total amount of calcium hydroxide is smaller for 10M samples only until the 3rd day of hydration. As it was measured and exemplified on Fig. 6, the higher degree of hydration found on samples with VMA is coming mainly from the water lost from 105 until 450 °C, corresponding to hydration products such as AFm and CSH.

Another important characteristic of samples where the viscosity modifier was employed is the total amount of calcium carbonate. The proportions from this mineral rise with the increasing employment of the admixture. To explain this result two hypothesis were raised. The first hypothesis considered that this carbonation happened during the TGA test. The second acknowledge that the total time needed for sample preparation before storing them in the freeze drier was enough to cause a certain level of carbonation.

According with the first hypothesis products formed during the heating up of the VMA would induce some carbonation in the samples. To test this hypotheses thermogravimetric tests were performed in calcium hydroxide and calcium hydroxide mixed with 1% by weight of VMA. The calcium hydroxyde used was supplied

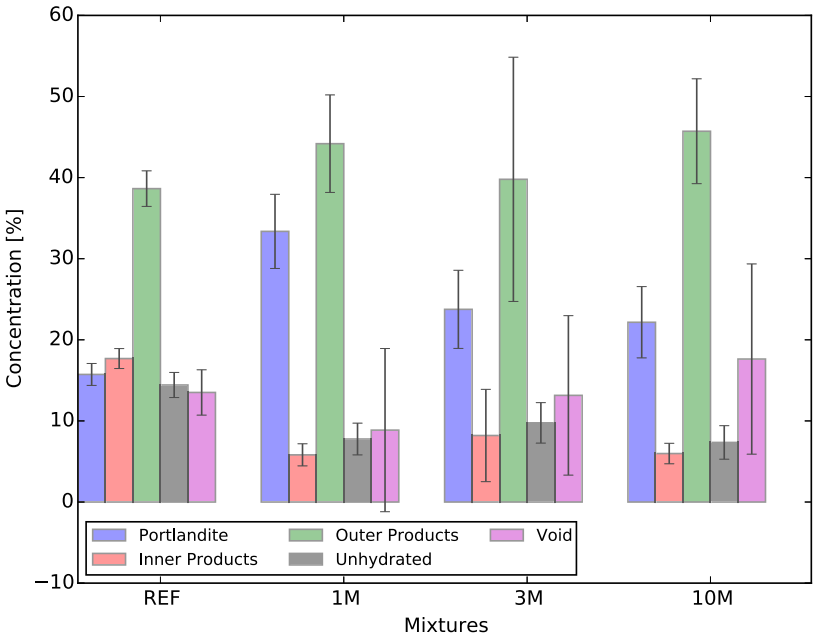

Fig. 13. Summary of the results from image analysis obtained from SEM images.

by VWR chemicals and according to the certificate of analysis provided by the manufacture the material employed should have a purity higher than 96%, and specifically for the lot used in this research 97% was measured. The goal was to emulate the same environment found during the TGA tests for the cement pastes but, with a much higher VMA-to-CH ratio. This high concentration of both components would hypothetically lead to a great formation of calcium carbonate.

Figs. 5(a) and 5(b) show the obtained TGA/ DTG curves and the summary of the total amount of calcium hydroxide and calcium carbonate found for this experiment respectively. As it can be seen, the calcium hydroxide levels were stable and the amount of calcium carbonate were slightly higher for samples with VMA. A consumption of $Ca(OH)_2$ was expected to generate the $CaCO_3$, and a much higher amount of the carbonated mineral was expected to be formed. Therefore, as a conclusion of this study it is possible to say that the higher content of calcium carbonate found for samples with VMA was not caused by a reaction between the CH and the products formed when VMA is submitted to high temperatures.

As the first hypothesis could not be validated, only the second hypothesis seams to explain this accelerated carbonation. This phenomenon might be correlated with the large amount of entrapped air voids found on samples with HPMC. Accelerated carbonation was previously reported for foamed concrete, as the total surface area exposed to the gas is larger [45]. The total amount of calcium carbonate in the cement used during this study was 1.22%. Therefore, carbonation happened for all samples with more emphasis on the samples with VMA. This phenomenon might be influenced by the combination of several factors: larger surface area of samples used for TGA (crushed particles of about 1 mm edge); significantly larger volume of air voids; and the abnormal precipitation of portlandite in the inner walls of the voids.

Assuming that the only source of calcium carbonate in those samples are coming from the original amount of filler in the cement and the rest was generated due to carbonation the last column of Table 2 shows how higher the total percentage of CH would be.

3.3. X-ray diffraction

The absence of some intermediate cement hydration minerals might be happening due to: delayed hydration due to VMA use; and the lack of distinguishment of the heat release peaks from ettringite and C_3S. Therefore, an investigation into the mineralogical composition was carried out in order to verify if the modal composition followed a similar trend in VMA containing samples as well as the REF ones.

In Fig. 7 the XRD pattern for samples with 29 days samples are shown. As the results were analysed only qualitatively, the patterns did not present formation of new or lack of minerals. Therefore, the employment of rheology modifier does not generate any hazardous minerals which could lead to a decrease on the durability or reliability of printed cementitious composites.

3.4. Fourier transform infrared spectroscopy

In Fig. 8 the FTIR results from 3 and 7 days samples are plotted to exemplify the hydration evolution and the differences among specimens with different VMA content. According with Singh et al., 2003 [46], the band corresponding to the presence of $Ca(OH)_2$ is found at 3645 cm^{-1} and from 1635 to 3445 cm^{-1} are bands due to the presence of calcium sulphate in the form of ettringite. Observing the figures corresponding to the first 1, 2 and 3 days of hydration, the presence of especially the bands corresponding to ettringite are very important.

As demonstrated with the calorimetry tests, the employment of VMA delays hydration of Portland cement. Therefore, especially the presence of these bands closely explains hydration evolution. 3M samples show higher transmittance bands, until the 3rd day of

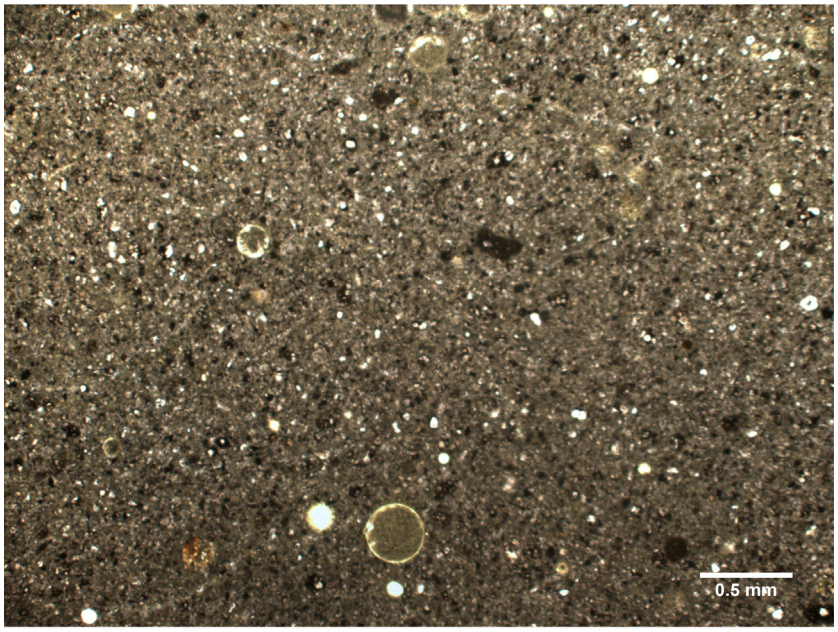

(a) REF sample in PPL

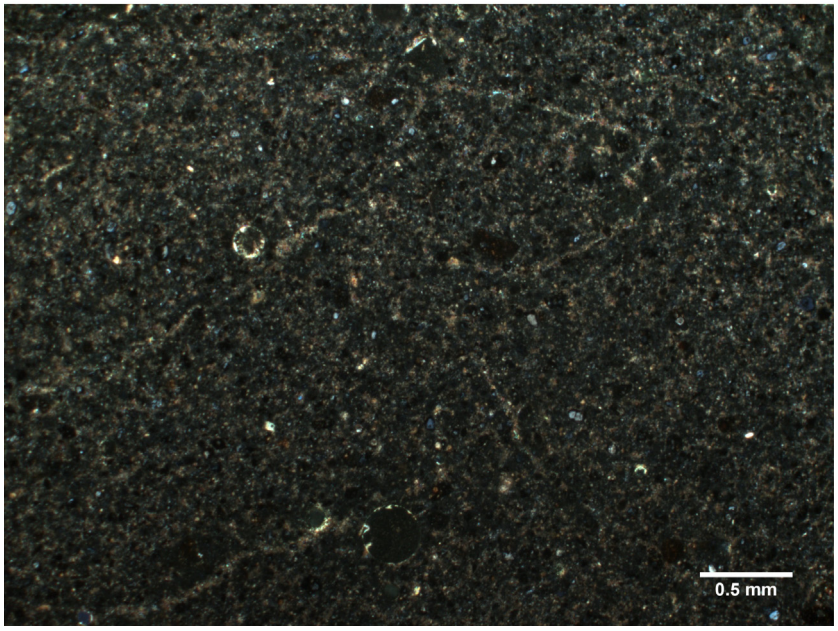

(b) REF sample in CPL

Fig. 14. Thin section images from REF samples.

hydration. Moreover, from the 7^{th} hydration day 10M samples took over, as the reactions for those samples were significantly delayed, like reported with the calorimetry results. The FTIR results followed the same trend observed in TGA and calorimetry test results.

3.5. Qualitative and quantitative image analysis

The microstructure of 29 days-old samples was observed under scanning electron microscope and are exemplified on Figs. 9(a), 10(a), 11(a) and 12(a). One of the first differences noticed was the number of voids in samples where the chemical admixture was used. This might be caused due to the high viscosity achieved while mixing the paste, which facilitated air entrapment.

Besides that, around the voids found on samples with VMA a higher capillary porosity region is always found, leading to the conclusion that these are less dense than the bulk paste. This means that the voids found on these samples were perhaps filled or at least highly concentrated with water. This is an important result that is connected to the fact that the HPMC molecules can 'arrest'

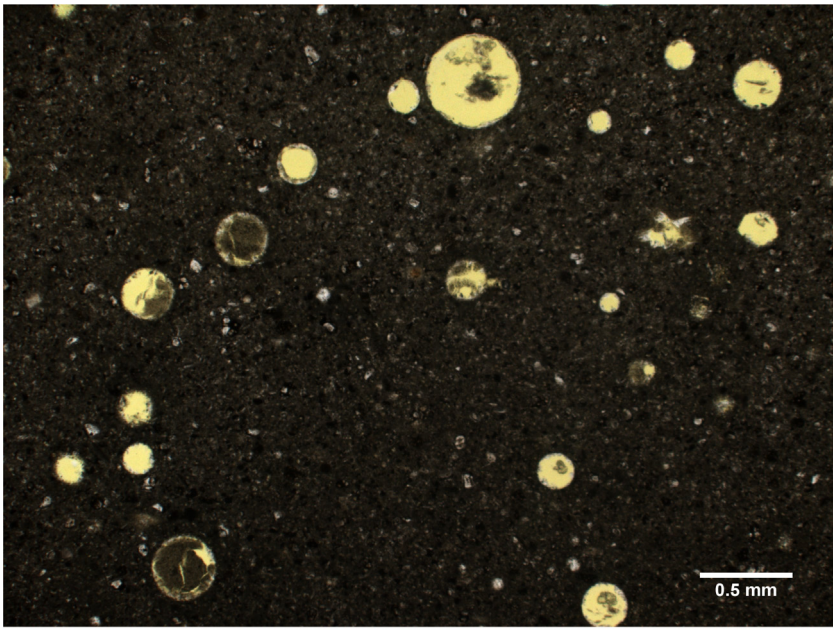

(a) 1M sample in PPL

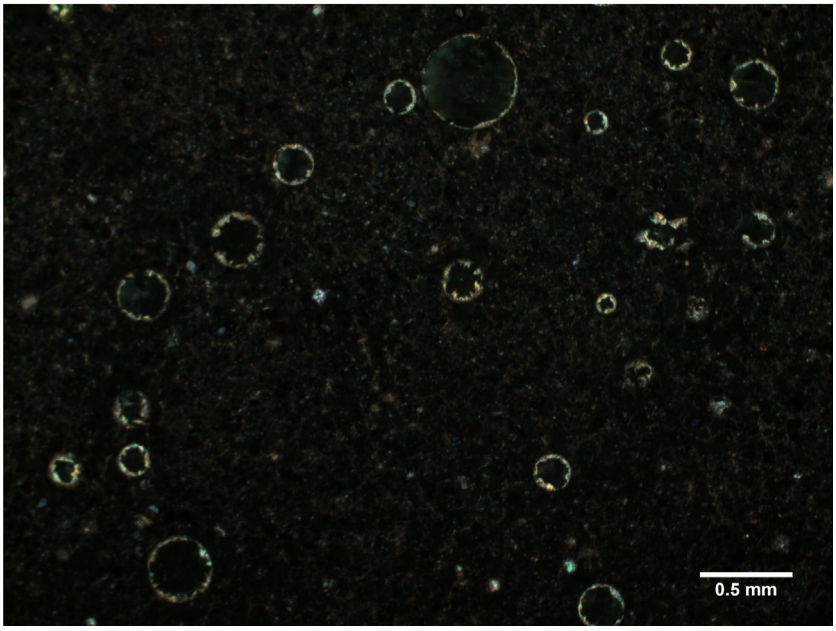

(b) 1M sample in CPL

Fig. 15. Thin section images from 1 M samples.

part of the mixing water through its -OH ramifications. As the hydration further progresses, the water molecules are released which contributes for the curing of the surrounding area.

Some examples from the image analysis performed on the SEM micrograph are shown in Figs. 9(b), 10(b), 11(b) and 12(b) summary of results obtained are shown on Fig. 13. They confirm a increasingly larger volume of voids found in specimens with VMA, as well as the decreasing total area of unhydrated OPC grains. However, the large standard deviation found for the void content makes clear the need of another technique to quantify this phase. In agreement with the results found on TGA and the accelerated carbonation hypothesis, large amount of calcium hydroxide was measured by image analysis. Results found with this technique were in agreement with an enhancement on Portland cement hydration whenever VMA is employed.

Another noteworthy observation was the location where portlandite clusters were found. Usually, $Ca(OH)_2$ grows disperse in the paste and eventually inside the void or pore walls. However, voids in VMA samples were progressively filled with portlandite, from 0.1 to 1 wt.% of VMA. It is important to notice, as mentioned in the introduction, that other research have already reported formation of portlandite with different morphology in cement pastes with VMA [20]. In order to illustrate this phenomena thin section photomicrograph, with 2.5× magnification, are shown on

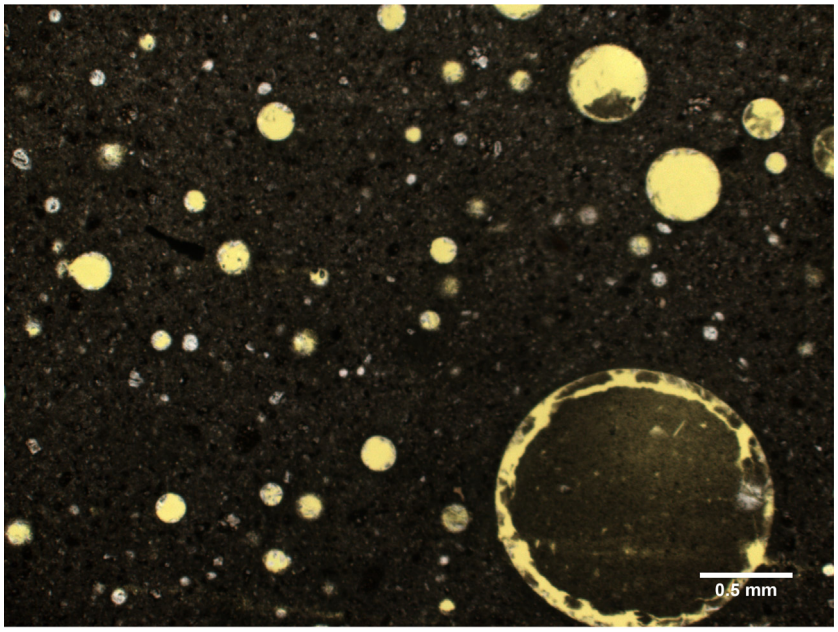

(a) 3M sample in PPL

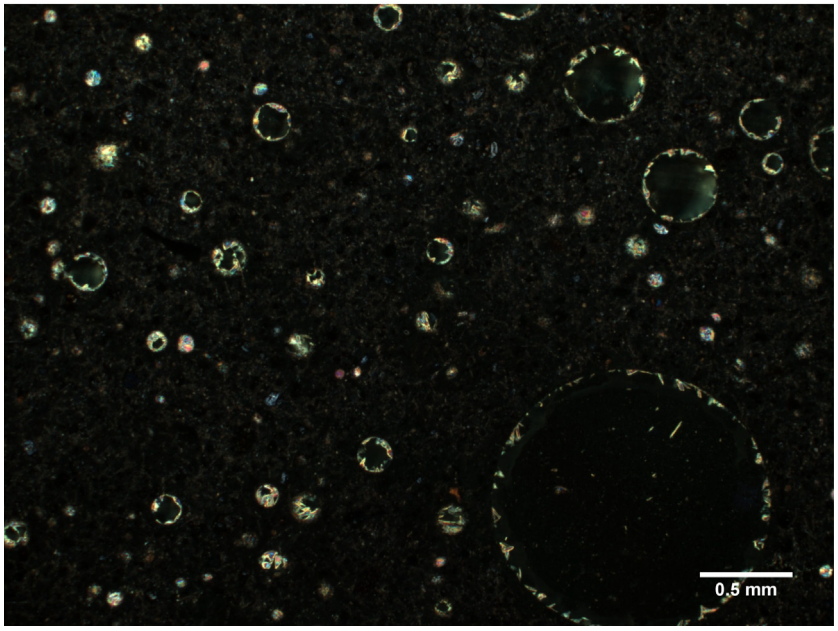

(b) 3M sample in CPL

Fig. 16. Thin section images from 3 M samples.

Figs. 14–17. Remarkably, voids from 10M samples were almost completely filled with portlandite, such as the ones showed in Fig. 18, with 20× magnification.

Employing images obtained from CT-scan the average void area and the average void diameter of the image stack from the studied paste are shown on Fig. 19. In order to avoid the influence of measurement noise, only voids larger than 5 pixels were taken into account during the measurements. Results obtained from this experiment demonstrate that not only the porosity increases with the employment of VMA but also the average size of these voids. Those results contribute to the explanation for the lower compressive strength obtained for mixture where the VMA is employed.

3.6. Rheology properties

The rheology parameters measured on the cement paste with HPMC can be found in Table 3 and 4. Using VMA did not seam to lead to a direct increase on the initial bulk yield stress (σ_0) but

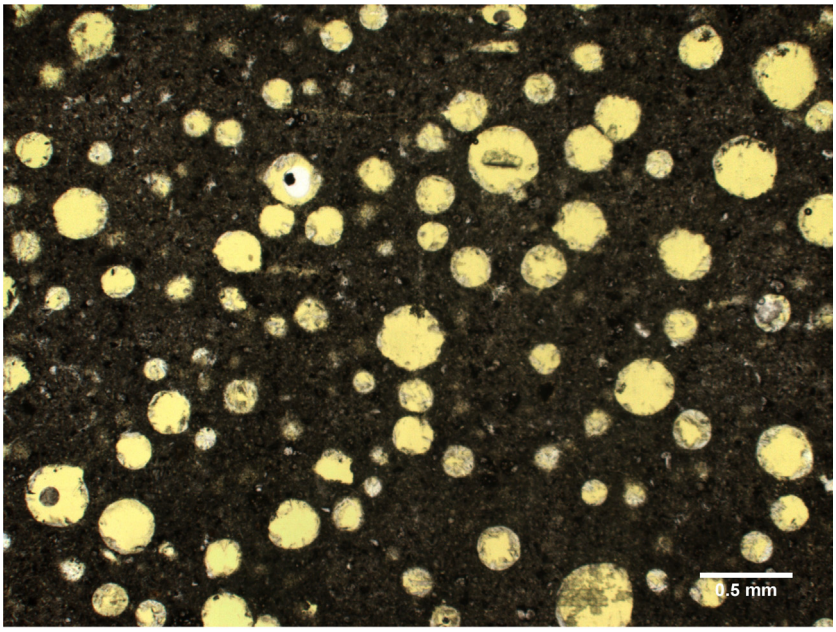

(a) 10M sample in PPL

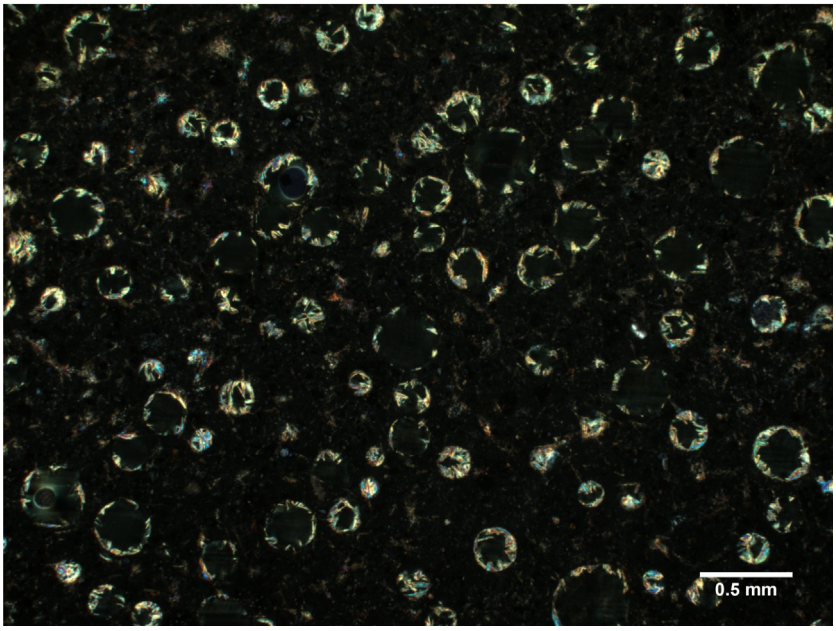

(b) 10M sample in CPL

Fig. 17. Thin section images from 10 M samples.

had an immediate effect on the initial shear yield stress (τ_0). This influence is more evident when the ratio between σ_0 and τ_0 is taken in account. This result together with the pictures (Fig. 20) emphasize the importance of VMA to achieve the needed rheology for 3D printing purposes. As the Benbow-Bridgwater equation with six parameters analysis was used to characterize the rheology parameters, the bulk dynamic stress (αV^m) and the shear dynamic stress (βV^n), for a given extrusion speed (which for this case was adopted 18 mm/s). Using the same parameters the extrusion pressure for each paste can be predicted, as shown on Table 4.

Using the same approach employed in [12] one can estimate that from all studied pastes, only 1M, 3M and 10M would be able to be printed. An extra conclusion could be drafted from the rheological experiments. Consider a printing layer with a rectangular cross section with 40 mm width and 10 mm height. Moreover, supposing a maximum theoretical density of 2100 kg/m^3 for the studied mixtures each printed layer will produce a hydrostatic pressure

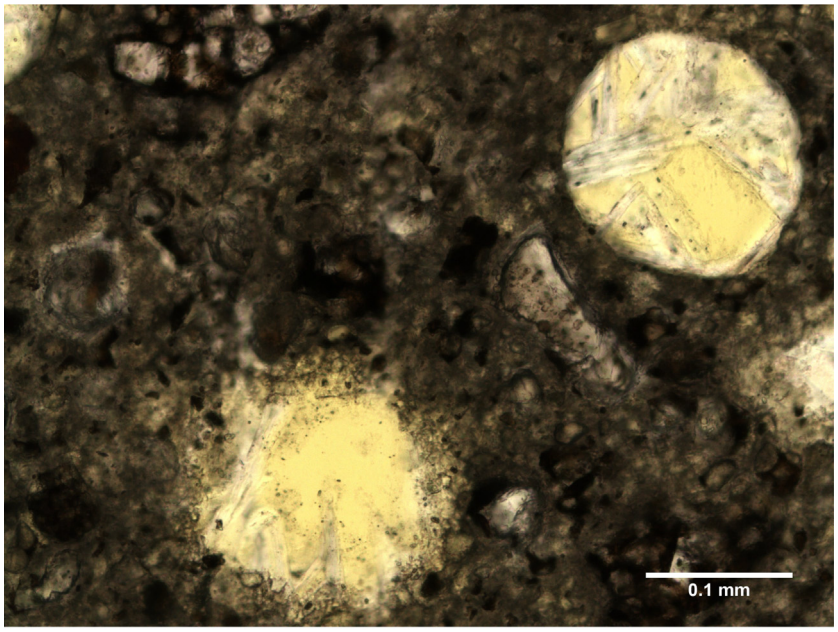

(a) 10M sample in PPL 20×

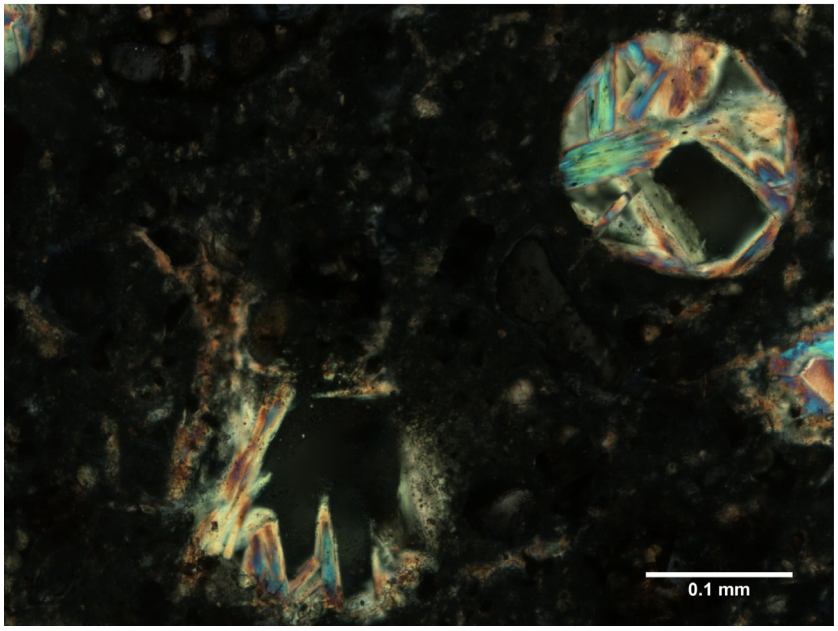

(b) 10M sample in CPL

Fig. 18. Thin section images from 10 M samples with 20× magnification.

of approximately 2 kPa. Therefore, among all studied mixtures only 1M, 3M and 10M would be considered printable and would be able to support approximately a maximum of 6, 6 and 11 layers, respectively.

3.7. Mechanical properties

The overall compressive strength for 2, 3, 7 and 29 days of curing decreases significantly as the weight percentage of VMA increases, as shown on Fig. 21. These results are aligned with the rise of the total volume and the average size of the air entrapped voids found on the samples. Therefore, any improvement on the OPC hydration provided by the internal curing when VMA is used cannot be quantified by means of mechanical performance at this scale. In order to investigate any improvement on the hydrated products a mechanical performance characterization at a smaller scale must be made. This investigation was possible using the nanoindentation results.

In Fig. 22(a) and (b) the Young's modulus frequency distribution and the frequency of some hydration products are given. It is known that the VMA percentage has a direct influence on the formation of hydration products, as it was already shown in the pre-

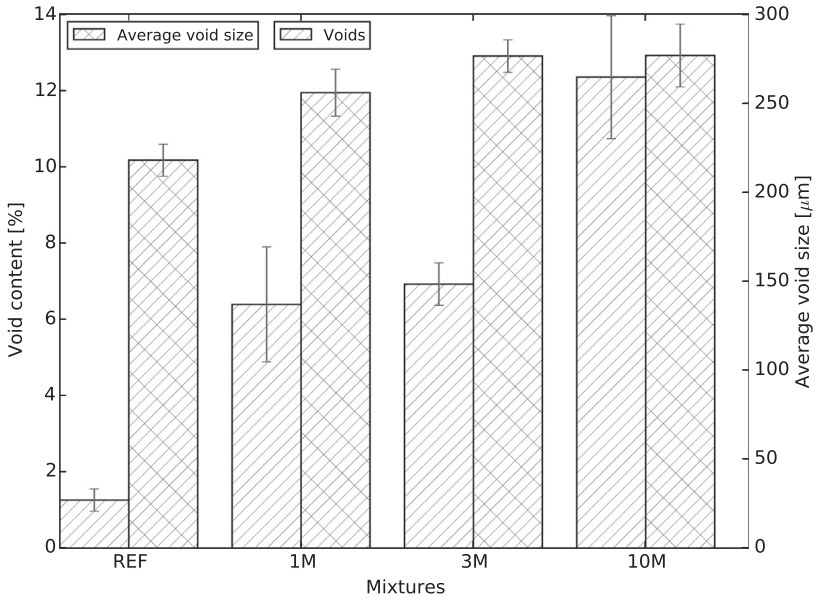

Fig. 19. Void content and average void diameter assessed by micro CT-scan.

Table 3
Summary of measured rheology parameters (First part).

Specimens	α [Kpa.s/mm]	β [Kpa.s/mm]	σ_0 [kPa]	τ_0 [kPa]
REF	1.631 ± 0.095	0.111 ± 0.001	16.313 ± 0.9637	0.200 ± 0.071
1 M	1.282 ± 0.108	0.160 ± 0.006	12.841 ± 1.086	0.636 ± 0.059
3 M	1.302 ± 0.116	0.181 ± 0.011	13.016 ± 1.170	0.828 ± 0.104
10 M	2.268 ± 0.255	0.474 ± 0.023	22.673 ± 2.545	2.372 ± 0.115

Table 4
Summary of measured rheology parameters (Second part).

Specimens	m	n	σ_0/τ_0	αV^m [kPa]	βV^n [kPa]	Pressure for V = 18 mm/s and L/D = 8 [kPa]
REF	0.42 ± 0.019	0.145 ± 0.031	81.46	5.49	0.17	59.72
1 M	0.349 ± 0.023	0.338 ± 0.026	20.19	3.52	0.42	69.87
3 M	0.353 ± 0.025	0.423 ± 0.047	15.73	3.61	0.61	82.69
10 M	0.54 ± 0.043	0.672 ± 0.014	9.56	10.81	3.31	255.36

(a) REF (b) 1M (c) 3M (d) 10M

Fig. 20. Visual difference on the shape stability of Portland cement paste with different VMA content after test in the ram extruder.

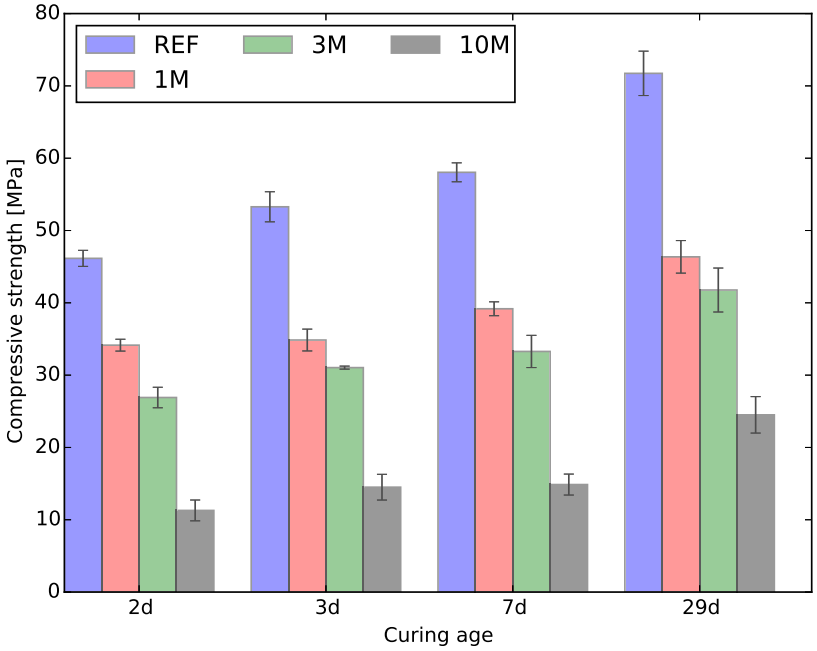

Fig. 21. Compressive strength development.

vious sections. For all samples with VMA the frequency appearances of indents on unhydrated particles was smaller than the reference sample. This result reinforces the argument that the VMA contributes to the hydration of cement, by means of internal curing.

Furthermore, the frequency of indents on portlandite was smaller than the reference for 3M and 10M samples. An immediately conclusion could be drafted saying that there is a smaller concentration of this mineral for these samples. However, observing the results found on the image analyses of SEM pictures and on the thin section images this conclusion would be disrupted. Therefore, all the results found here on this study lead the authors to confirm that the portlandite precipitation on samples with high content of VMA has an abnormal behaviour. The $Ca(OH)_2$ distribution on samples with VMA is very different than an ordinary cement paste. In 3M and 10M samples the portlandite crystals precipitates more often on the air void inner walls and not spread on the bulk of the cement paste. This abnormal precipitation of portlandite might be specifically related with the different viscosity that samples with VMA show, and quantified by the σ_0/τ_0 ratio on Table 4. In addition, this might lead to an increased Ca^{+2} leaching from the pore solution towards the entrapped air voids. This type of behaviour is not shown in concrete with air entrainment admixtures as the viscosity of the liquid phase (excluding the air voids) of this type of material does not change, for example.

4. Conclusions

The results obtained during this study were important for the understanding of the influence of using VMA on cementitious materials. A wide range of industries make use of this chemical admixture, such as those that extrude fibre reinforced cementitious composites and nowadays additive manufacturing based on extrusion. Summarizing the main conclusions are:

- Rheological properties of cementitious materials using VMA are significantly different than the ordinary ones. The employment of the admixture brings shape stability and guarantee higher initial bulk yield stresses which is essential for extrusion based 3d printing;
- VMA concentration is of high importance on OPC hydration. Even small concentrations of the admixture lead to retardation of the initial hydration. 1 wt.% already leads to a large latent time of the Portland cement;
- It is likely that the rheology modifier admixture ‘arrests’ the available water with hydrogen bonds. The admixture only loses its preference for the water when the pH of the solution increases, making stronger connections with other ions;
- As demonstrated with the degree of hydration and the total heat released VMA can also be employed for internal curing purposes;
- Under electron microscope, it was possible to observe that entrapped air voids formed during mixing works also as water reservoir. As soon as the pH of the paste rises, the water released from VMA develops a region around theses voids with a higher water/cement ratio, in comparison with the rest of the matrix;
- To modify the rheology parameters of solid suspensions, the grain size distribution or the employment of viscosity modifier admixtures are usually employed. However, the results found in this research suggest that VMA loses its preference for H_2O molecules when enough OH^- ions are available in solution. Therefore, solid suspensions which have high pH from the beginning of the mixing, such as alkali activated materials, will be challenged to decrease the solution’s pH or provide a well distributed particles grain size.
- The employment of VMA changes the portlandite growing mechanism on Portland cement pastes. Samples with VMA show an abnormal preferential grow of $Ca(OH)_2$ crystals on the internal walls of the entrapped air voids, most probably suggesting that these samples are more exposed to Ca^{+2} leaching from the pore solution to the entrapped air voids.

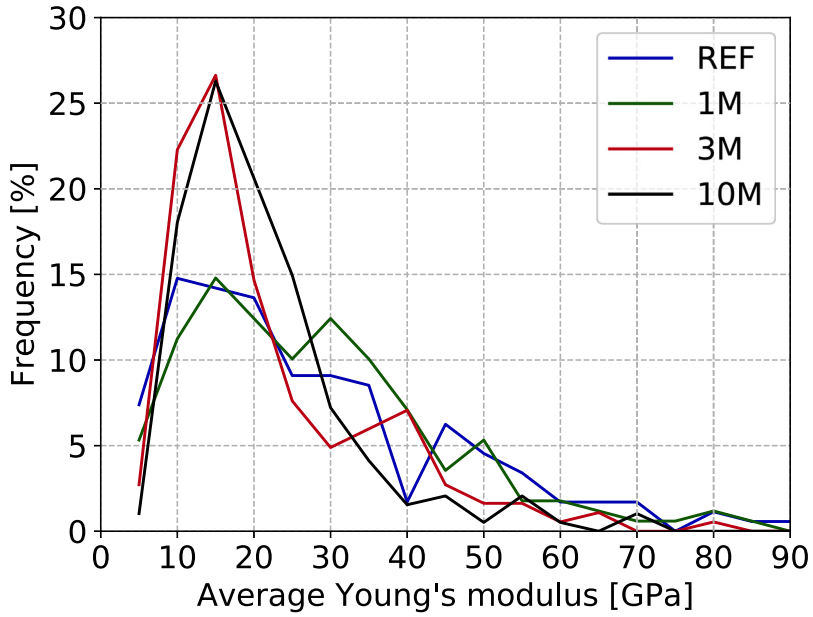

(a) Frequency distribution of Young's modulus assessed by nanoindentention

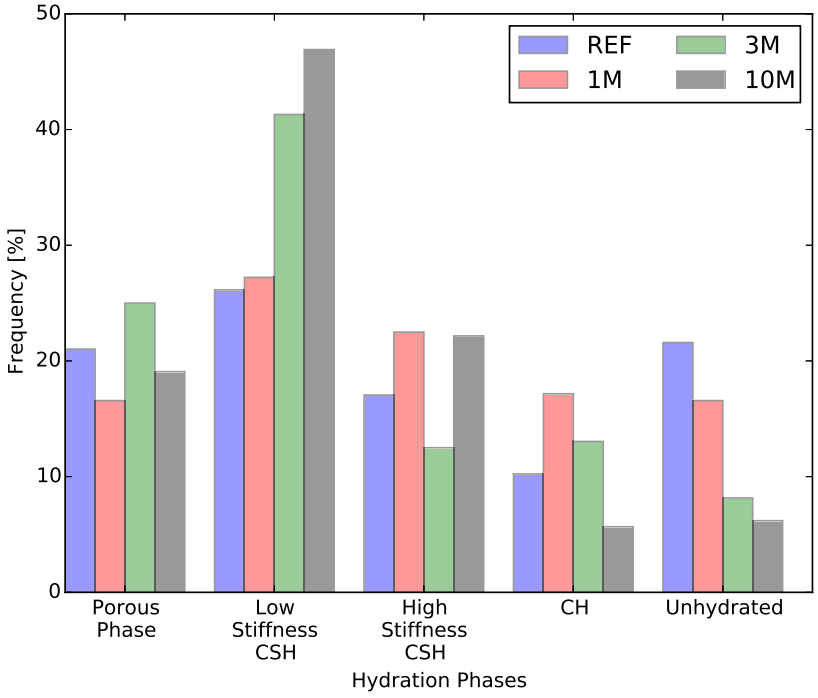

(b) Frequency of some OPC hydration products

Fig. 22. Nanoindentation results.

Conflicts of interest

None.

Acknowledgements

The authors would like to acknowledge the funding from Science Without Borders from the National Council for Scientific and Technological Development of Brazil (201620/2014-6).

References

[1] P. Wu, J. Wang, X. Wang, A critical review of the use of 3-D printing in the construction industry, Autom. Constr. 68 (2016) 21–31.
[2] H. Kodama, Automatic method for fabricating a three-dimensional plastic model with photo-hardening polymer, Rev. Sci. Instrum. 52 (11) (1981) 1770–1773.
[3] E. Sachs, M. Cima, J. Cornie, D. Brancazio, J. Bredt, A. Curodeau, T. Fan, S. Khanuja, A. Lauder, J. Lee, S. Michaels, Three-dimensional printing: the physics and implications of additive manufacturing, CIRP Ann. – Manuf. Technol. 42 (1) (1993) 257–260.
[4] R.A. Buswell, R.C. Soar, A.G.F. Gibb, A. Thorpe, Freeform construction: mega-scale rapid manufacturing for construction, Autom. Constr. 16 (2) (2007) 224–231.

[5] J. Wilkes, Y. Hagedorn, W. Meiners, K. Wissenbach, Additive manufacturing of ZrO_2-Al_2O_3 ceramic components by selective laser melting, Rapid Prototyping J. 19 (1) (2013) 51–57.
[6] B. Khoshnevis, Automated construction by contour crafting – Related robotics and information technologies, Autom. Constr. 13 (1) (2004) 5–19.
[7] F. Bos, R. Wolfs, Z. Ahmed, T. Salet, Additive manufacturing of concrete in construction: potentials and challenges of 3D concrete printing, Virtual Phys. Prototyping 11 (3) (2016) 209–225.
[8] A. Kazemian, X. Yuan, E. Cochran, B. Khoshnevis, Cementitious materials for construction-scale 3D printing: Laboratory testing of fresh printing mixture, Constr. Build. Mater. 145 (2017) 639–647.
[9] F.P. Bos, Z.Y. Ahmed, E.R. Jutinov, T.A. Salet, Experimental exploration of metal cable as reinforcement in 3D printed concrete, Materials 10 (11) (2017).
[10] V.C. Li, H. Horii, P. Kabele, T. Kanda, Y. Lim, Repair and retrofit with engineered cementitious composites, Eng. Fract. Mech. 65 (2–3) (2000) 317–334.
[11] T. Kamada, V.C. Li, Effects of surface preparation on the fracture behavior of ECC/concrete repair system, Cem. Concr. Compos. 22 (6) (2000) 423–431.
[12] S.C. Figueiredo, C.R. Rodríguez, Z.Y. Ahmed, D. Bos, Y. Xu, T.M. Salet, O. Çopurog ˘lu, E. Schlangen, F.P. Bos, An approach to develop printable strain hardening cementitious composites, Mater. Des. 169 (2019) 107651.
[13] S. Srinivasan, D. Deford, P. Shah, The use of extrusion rheometry in the development of extrudate fibre-reinforced cement composites, Concr. Sci. Eng. 1 (11) (1999) 26–36.
[14] K.H. Khayat, Viscosity-enhancing admixtures for cement-based materials an overview, Cem. Concr. Compos. 20 (2) (1998) 171–188.
[15] L. Patural, P. Marchal, A. Govin, P. Grosseau, B. Ruot, O. Devès, Cellulose ethers influence on water retention and consistency in cement-based mortars, Cem. Concr. Res. 41 (1) (2011) 46–55.
[16] D. Bülichen, J. Kainz, J. Plank, Working mechanism of methyl hydroxyethyl cellulose (MHEC) as water retention agent, Cem. Concr. Res. 42 (7) (2012) 953–959.
[17] A. Pierre, A. Perrot, V. Picandet, Y. Guevel, Cellulose ethers and cement paste permeability, Cem. Concr. Res. 72 (2015) 117–127.
[18] C. Brumaud, R. Baumann, M. Schmitz, M. Radler, N. Roussel, Cellulose ethers and yield stress of cement pastes, Cem. Concr. Res. 55 (2014) 14–21.
[19] D. Marchon, S. Kawashima, H. Bessaies-Bey, S. Mantellato, S. Ng, Hydration and rheology control of concrete for digital fabrication: Potential admixtures and cement chemistry, Cement Concr. Res. 112 (2018) 96–110. SI: Digital concrete 2018.
[20] E. Knapen, D. Van Gemert, Cement hydration and microstructure formation in the presence of water-soluble polymers, Cem. Concr. Res. 39 (1) (2009) 6–13.
[21] P. Pichniarczyk, G. Malata, Microcalorimetric analysis of methylcellulose influence on the hydration process of tricalcium aluminate, alite and their mixture, J. Therm. Anal. Calorim. 128 (2) (2017) 771–778.
[22] J. Pourchez, A. Peschard, P. Grosseau, R. Guyonnet, B. Guilhot, F. Vallée, HPMC and HEMC influence on cement hydration, Cem. Concr. Res. 36 (2) (2006) 288–294.
[23] J. Pourchez, P. Grosseau, B. Ruot, Current understanding of cellulose ethers impact on the hydration of C3A and C3A-sulphate systems, Cem. Concr. Res. 39 (8) (2009) 664–669.
[24] J. Pourchez, P. Grosseau, B. Ruot, Changes in C3S hydration in the presence of cellulose ethers, Cem. Concr. Res. 40 (2) (2010) 179–188.
[25] Z.H. Ou, B.G. Ma, S.W. Jian, Influence of cellulose ethers molecular parameters on hydration kinetics of Portland cement at early ages, Constr. Build. Mater. 33 (2012) 78–83.
[26] B. Ma, Y. Peng, H. Tan, S. Jian, Z. Zhi, Y. Guo, H. Qi, T. Zhang, X. He, Effect of hydroxypropyl-methyl cellulose ether on rheology of cement paste plasticized by polycarboxylate superplasticizer, Constr. Build. Mater. 160 (2018) 341–350.
[27] B. Wu, G. Ye, Development of porosity of cement paste blended with supplementary cementitious materials after carbonation, Constr. Build. Mater. 145 (2017) 52–61.
[28] P. Lura, Autogenous Deformation and Internal Curing of Concrete, Delft University of Technology, 2003. PhD thesis.
[29] J. Zhang, G.W. Scherer, Comparison of methods for arresting hydration of cement, Cem. Concr. Res. 41 (10) (2011) 1024–1036.
[30] O. Çopuroğlu, Revealing the dark side of portlandite clusters in cement paste by circular polarization microscopy, Materials 9 (3) (2016).
[31] I. Arganda-carreras, V. Kaynig, C. Rueden, K.W. Eliceiri, J. Schindelin, A. Cardona, H.S. Seung, Trainable Weka Segmentation: a machine learning tool for microscopy pixel classification, Bioinformatics 33 (March) (2017) 2424–2426.
[32] J. Schindelin, I. Arganda-carreras, E. Frise, V. Kaynig, T. Pietzsch, S. Preibisch, C. Rueden, S. Saalfeld, B. Schmid, J.-Y. Tinevez, D.J. White, V. Hartenstein, P. Tomancak, A. Cardona, Fiji – an Open Source platform for biological image analysis, Nat. Methods 9 (7) (2012) 676–682.
[33] M.S. Konsta-Gdoutos, Z.S. Metaxa, S.P. Shah, Multi-scale mechanical and fracture characteristics and early-age strain capacity of high performance carbon nanotube/cement nanocomposites, Cement Concr. Compos. 32 (2) (2010) 110–115.
[34] M.S. Konsta-Gdoutos, Z.S. Metaxa, S.P. Shah, Highly dispersed carbon nanotube reinforced cement based materials, Cem. Concr. Res. 40 (7) (2010) 1052–1059.
[35] A.K. Suryavanshi, J.D. Scantlebury, S.B. Lyon, Mechanism of Friedel's salt formation in cements rich in tri-calcium aluminate, Cem. Concr. Res. 26 (5) (1996) 717–727.
[36] F.R. Lago, J. Dweck, T. Analysis, Evaluation of influence of salt in the cement hydration to oil wells, Materials Res. 20 (2017) 743–747.
[37] B. Šavija and E. Schlangen, "Chloride ingress in cracked concrete- a literature review," in Advances in Modeling Concrete Service Life (C. Andrade and J. Gulikers, eds.), (Dordrecht), pp. 133–142, Springer Netherlands, 2012.
[38] B. Šavija, J. Pacheco, E. Schlangen, Lattice modeling of chloride diffusion in sound and cracked concrete, Cement Concr. Compos. 42 (2013) 30–40.
[39] H.F.W. Taylor, Cement Chemistry, Academic Press, 1990.
[40] A. Mezencevova, V. Garas, H. Nanko, K.E. Kurtis, Influence of thermomechanical pulp fiber compositions on internal curing of cementitious materials, J. Mater. Civ. Eng. 24 (8) (2012) 970–975.
[41] P. Jongvisuttisun, C. Negrello, K.E. Kurtis, Effect of processing variables on efficiency of eucalyptus pulps for internal curing, Cement Concr. Compos. 37 (2013) 126–135.
[42] D. Shen, X. Wang, D. Cheng, J. Zhang, G. Jiang, Effect of internal curing with super absorbent polymers on autogenous shrinkage of concrete at early age, Constr. Build. Mater. 106 (2016) 512–522.
[43] D. Zou, H. Zhang, Y. Wang, J. Zhu, X. Guan, Internal curing of mortar with low water to cementitious materials ratio using a normal weight porous aggregate, Constr. Build. Mater. 96 (2015) 209–216.
[44] A. Bentur, S. ichi Igarashi, K. Kovler, Prevention of autogenous shrinkage in high-strength concrete by internal curing using wet lightweight aggregates, Cem. Concr. Res. 31 (11) (2001) 1587–1591.
[45] E. Namsone, G. Šahmenko, A. Korjakins, Durability properties of high performance foamed concrete, Procedia Eng. 172 (2017) 760–767.
[46] N.K. Singh, P.C. Mishra, V.K. Singh, K.K. Narang, Effects of hydroxyethyl cellulose and oxalic acid on the properties of cement, Cem. Concr. Res. 33 (9) (2003) 1319–1329.